國立臺灣大學理學院大氣科學研究所

碩士論文

Department of Atmospheric Sciences

College of Science

National Taiwan University

Master Thesis

熱帶氣旋生成類型及其增強速率之探討

On Tropical Cyclone Genesis Types and Their Intensification Rate

鍾明翰

Ming-Han Chung

指導教授：吳俊傑 博士

Advisor: Chun-Chieh Wu, Ph.D.

中華民國 112 年 8 月

August 2023

致謝

　　這是一條既順遂又艱辛的道路，自從我在幼稚園時期對颱風感興趣開始，人生彷彿已有固定的方向。首先感謝吳俊傑老師提供機會，讓我成為颱風動力研究室的一份子，並提供優渥的研究環境，使我能自由發揮靈感和依照自己的步調投入研究，令我得以熟悉大氣領域的研究與學者，也令我得以認識到研究室內的各位颱風迷。感謝研究室各夥伴的支援，在每次 seminar 前以及 group meeting 時一起充分討論大氣研究，在每次會議結束後一起充分閒聊大氣界趣事亦或是認真探討雙眼牆觀測，在每次颱風警報期間充分討論颱風結構、發展、路徑與地形效應(即便颱風都沒有登陸臺灣)。在此感謝怡瑄學姊、禹安學長、約禮學長，對我的研究提供充分的協助，並對我的研究方法提供充分的見解，使我的研究更加嚴謹。也感謝忠權學長、自雄學長、Peter 學長、金成學長、里治學長處理研究室事務以及提供研究看法，讓我的研究工作更加得心應手。接著感謝宗勇學長、欽旋學長、宜萱學姊、宜臻學姊、顥瑄學姊、國峰學長，與其他離開研究室的學長姐，提供研究上的觀點及經驗上的分享。感謝浩廷學長、峻愷、Benjamin、俊宇、先嶸、昱丞、柏智參與研究室的各種討論，為彼此的研究提供非常多重要的建議，也一同創造歡樂的研究室生活。特別感謝同屆的峻愷與 Benjamin 同學，提供許多學務上的資訊，協助指導各種表格的填寫。也感謝禹安學長在世紀帝國二的出兵協助，以及約禮學長與浩廷學長在城市天際線的城市規劃交流。

　　同時也感謝非常多研究室以外的諸位貴人協助。感謝茂正學長、詣軒、建泓以及其他一同吃晚餐的夥伴，在晚餐前閒聊許多天氣系統，提供我大量的研究靈感。Special thanks to Prof. Griffith for his guidance in thesis writing during the class. 感謝鄧旭峰研究員在我研究初期提供想法，與擔任口試委員審查我的研究，也感謝連國淵老師擔任我的口試委員。兩位委員提出的問題與建議，都讓我的研究更加嚴謹。感謝清大統計所朋友李丞恩，提供統計檢定方面的建議。感謝大學同學劉景岳，詢問我的研究圖表中的特徵，協助我將研究結果用文字表達出來。感謝其他在中央或臺大認識的朋友們，不管是學長姐、同學亦或是學弟妹，感謝各位在需要的時候陪我散散心，感謝你們的陪伴。也非常感謝在中央或臺大認識的各位教授，各位教授的付出，不管是課程教學亦或是指導專題研究都成就了我，讓我在中央的大學四年與在臺大的碩士兩年均有很大的收穫。最後，誠摯的感謝我的家人，不斷支持我通往大氣系的道路，我能深刻感受到，在人生的道路上，能有家人支持自己的選擇，是很幸福的事。感謝各位，讓我們在未來，一同讓彼此更加快樂與滿足！

摘要

基於切向風收支方程，較小的最大風速半徑（RMW）會造成較高的熱帶氣旋（TC）增強速率。再者，RMW 內持續的對流會導致 RMW 收縮。因此，了解影響對流分布與 RMW 的因素，對於探討 TC 的增強速率至關重要。前人研究已顯示對流分布受 TC 生成類型的影響。然而，對 TC 生成的主觀分類難以代表其資料分布。本研究開發一種新的客觀方法，利用 ECMWF Reanalysis v5（ERA5）資料中挑選數個大氣參數，再運用 K-means 分群演算法對 TC 的生成類型做分類。為了比較增強速率和 RMW 之間的關係，本研究計算了每個個案的生命期最大增強速率（LMIR）。

本研究結果顯示 LMIR 與 RMW 之間接近反比關係，與前人研究一致。另外，在成為熱帶風暴（TS）時，具有較大 RMW 的 TC 通常具有較低的 LMIR，代表初始 RMW 也會影響 LMIR。K-means 分群分析顯示四種 TC 生成類型：(i) 季風匯流（MC）、(ii) 東風波（EW）、(iii) 季風風切（MS）、(iv) 季風低壓（MD）。相較於前人研究較不顯著的對流分布，此新方法的分類結果顯示，每個 TC 生成類型的對流分布呈現明顯差異，代表此新方法在區分 TC 生成時的結構上更有效。本研究的分類結果顯示，EW 的對流僅出現在中心周圍，MC 跟 MS 的對流雖然也集中在中心周圍，但 MC 外圍的對流往南延伸，而 MS 外圍的對流則是往東西兩側延伸，MD 的對流最為分散。由於 MD 的環流較大且對流分散，其 RMW 明顯較大，而 LMIR 較低，與 EW 相比具有統計顯著差異（Conover's test）。相反地，在 EW 個案，比濕較高和亮溫較低的區域均集中在中心周圍，這解釋了為何 EW 具有較小的 RMW。即使 MC 和 MS 的 RMW 大小介於 EW 和 MD 之間，但由於集中在中心的對流，它們的 LMIR 與 EW 相近。

在準理想實驗中，EW 較小的 RMW 明顯造成更高的渦度，因此根據切向風收支方程，EW 的增強速率高於 MD。儘管 MD 的 RMW 不斷收縮，但仍然具有較大的 RMW。在 RMW 一邊收縮，強度一邊增強的過程，其 RMW 周圍的切向風徑向曲率也不斷變大，代表 RMW 位置與其內側的風速差異變大，限制了 RMW 內側的風速上升至超過 RMW 位置風速的機會，造成 MD 的 RMW 無法繼續收縮。

關鍵字：熱帶氣旋生成、東風波、季風低壓、K-means 分群演算法、增強速率

Abstract
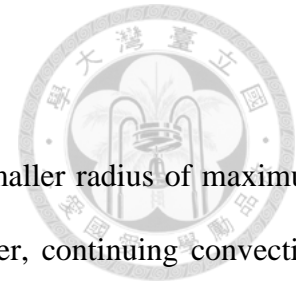
Higher tropical cyclone (TC) intensification rates are affected by smaller radius of maximum wind (RMW) based on the tangential wind tendency equation. Moreover, continuing convection within the RMW can cause RMW contraction. Thus, understanding the factors affecting convection distribution and RMW is crucial for characterizing TC intensification rates. Previous studies have shown that convection distribution is affected by TC genesis type. However, subjective classification of TC genesis does not rely on data distribution. In this study, a new objective method is developed to classify TC genesis type based on K-means clustering algorithm of critical atmospheric parameters available in ECMWF Reanalysis v5 (ERA5) data. For comparison between intensification rate and RMW, the lifetime maximum intensification rate (LMIR) in each case is also examined.

The result shows a nearly inverse proportion between the LMIR and RMW, which is consistent with previous research. In addition, TCs with larger RMW upon becoming a tropical storm (TS) usually have lower LMIR, implying that the initial RMW can also affect LMIR. The K-means cluster analysis shows four TC genesis types: (i) monsoon confluence (MC), (ii) easterly wave (EW), (iii) monsoon shear (MS), and (iv) monsoon depression (MD). The convection distribution shows a distinct difference in each genesis type, which is not so significant in previous studies, implying that this new method is more effective in distinguishing the structure of TCs. As a result of this new classification, EW has the most aggregated convection. Although MC and MS also have aggregated convection around TC center, the convection in outer region extends southward in MC and extends eastward and westward in MS. In contrast, MD has more scattered convection than others. Owing to larger circulation and scattered convection, MD has a significantly larger RMW and lower LMIR than EW (Conover's test). In contrast, EW cases have higher specific humidity and lower brightness temperature only around the center, explaining why EW has a small RMW. Although both MC and

MS have medium RMW sizes between EW and MD, their LMIR is as high as that in EW because of aggregated convection similar to EW.
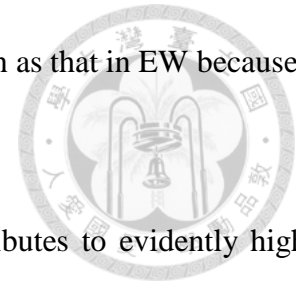
In the quasi-idealized experiment, the smaller RMW of EW contributes to evidently higher vorticity, thus EW has a higher intensification rate than MD based on the tangential wind tendency equation. Despite the continuous RMW contraction in MD, it still has a larger RMW than EW. During the period of RMW contraction and intensification, the radial curvature of tangential wind around RMW also increases. This indicates that the wind speed difference between RMW and its inner side increases, limiting the probability of wind speed inside RMW surpassing that at the RMW. Consequently, it stops the RMW contraction in MD.

Table of contents

List of Tables

List of Figures

Chapter 1

Introduction

1.1 The factors of TC intensification rate

Predicting tropical cyclone (TC) intensification rates (IRs) accurately is challenging, as they are influenced by (i) environmental factors, e.g. sea surface temperature (SST), vertical wind shear (VWS), relative humidity (RH), and (ii) inner-core dynamics, e.g. radius of maximum wind (RMW) (Carrasco et al. 2014; Xu and Wang 2018a; Li et al. 2021; Wu and Ruan 2021). Due to the high correlation between the inner core structure and intensity, when these factors affect the inner core structure of TC during the intensification period, the IR will change either (Wang and Wu 2004). To keep going on improving the forecast skill of the IR of TC, it is vital to figure out the different factors that influence IR.

1.1.1 The role of environmental factors

Environmental factors including the SST, VWS, and RH affect the IR through different processes. The influence of SST on the TC has been discussed in many studies (Emanuel 1988; Wang et al. 2021). Emanuel (1988) shows a theory of the potential intensity of TC in different environment, which tells us important information: the potential intensity of TC is infiuenced by the SST. Over the next thirty years, this theory has been optimized as the maximum potential intensity (MPI) theory (Wang and Wu 2004). Not only the intensity, but also the theory of IR has been derived from the MPI

theory. Wang et al. (2021) proposes a theory of the IR which is influenced by the SST and proven by the numerical model, suggesting that the higher SST causes the higher IR.

In addition, the VWS also affects IR by changing the inner core structure of TC. According to previous studies, higher VWS leads to the weakening of TC by advecting latent heat away from the low-level TC center (Wang and Wu 2004). Also, Wang et al. (2015) demonstrates a negative correlation between the VWS and the IR, and shows that TC tends to intensify with the VWS under 7 to 9 ms^{-1}. It seems that the VWS equals to 0 cause the highest IR, but this condition is rare in the real world. Furthermore, the data of intensity change spread widely in a low-VWS environment (Wang et al. 2015), which means that TC may weaken instead of intensification in a low-VWS environment. Therefore, there are still other factors affecting the IR.

The RH in upper level (500-300 hPa) around TC can change the IR by influencing the deep convection in the inner core of TC (Knaff et al. 2005). They also show that fast translation speed increases the IR. Although many environmental factors affect the IR and they can be well captured in the statistical model and the numerical model, the inner-core dynamic factors are still unknown as the results of models does not always match the observations (Rogers et al. 2017). Thus, researching the role of inner-core factors is needed.

1.1.2 The role of TC inner-core dynamic factors

The TC inner-core dynamic factors include the vortex Rossby waves, mesoscale vortices, deep eyewall clouds, and RMW (Wang and Wu 2004). In recent studies, the RMW is an important inner-core dynamic factor that influence the IR (Xu and Wang 2010, 2015, 2018a,b; Li and Wang 2021; Wu and Ruan 2021). The RMW-IR relationship

2

has been established with the tangential wind tendency equation. The original equation

of the azimuthal-mean tangential wind tendency is showing blow (Huang et al. 2018):

$$\frac{\partial \bar{V}}{\partial t} = -\bar{u}\bar{\zeta_a} - \bar{w}\frac{\partial \bar{V}}{\partial z} - \overline{u'\zeta_a'} - \overline{w'\frac{\partial V'}{\partial z}} - \overline{\frac{1}{\rho r}\frac{\partial P'}{\partial \lambda}} + \bar{F}_\lambda \quad (1\text{-}1)$$
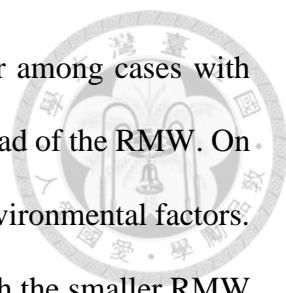
Where the u, V, w, overline symbol and apostrophe imply the radial wind, tangential wind,

vertical velocity, azimuthal-mean and asymmetric components, respectively. ζ_a

represents the absolute vorticity, which is composed of the curvature vorticity, shear

vorticity, and planetary vorticity.

In the azimuthal-mean framework, Li et al. (2021) derive the tangential wind

tendency equation at the RMW, which can represent the intensification rate. In their

framework, the Eq. 1-1 changes to:

$$\frac{\partial \overline{V_m}}{\partial \tau} = -\overline{u_m}\left(\frac{\overline{V_m}}{R_m} + \overline{f_m}\right) - \overline{w_m}\frac{\partial \overline{V_m}}{\partial z} + \overline{F_m} \quad (1\text{-}2)$$

Thus, the asymmetric components vanish in the azimuthal-mean model. Also, the shear

vorticity equals 0 at the RMW. The "τ" and subscript "m" implies the time and value at

the R_m, such as RMW, respectively. The left-hand side represents the IR. The first term

in right-hand side is the radial fluxes of absolute vorticity, which term shows a positive

contribution to the budget during intensification. The second and third terms on the right-

hand side represent the vertical advection of tangential velocity and surface friction and

subgrid-scale diffusion, respectively. Both of them are mostly negative contribution.

According to the tangential wind tendency equation, the higher IR is caused by

smaller RMW through the stronger curvature vorticity flux, and this phenomenon has

been observed in previous studies (Carrasco et al. 2014; Xu and Wang 2015, 2018a). In

the result of these previous studies using best-track data, there is a negative relationship

between the RMW and IR. However, the correlation is still unclear among cases with lower IR, which may be affected by other environmental factors instead of the RMW. On the other hand, numerical experiments can avoid the disruption of environmental factors. The numerical models also show the higher IR in the experiment with the smaller RMW (Xu and Wang 2010; Stern et al. 2015; Li and Wang 2021). Thus, smaller RMW causing higher IR is widely recognized.

Furthermore, continuing convection within the RMW can cause contraction and decrease the RMW (Stern et al. 2015; Li et al. 2019; Wu and Ruan 2021). By the conception model in Wu and Ruan (2021), the convective heating induces radial inflow outside the convection area. According to the Eq. 1-1, the radial inflow accelerates tangential wind through the radial vorticity flux. Thus, the convection near TC center can increase the tangential wind inside RMW and cause RMW contraction. Also, either stronger convection or smaller RMW is beneficial for intensifying. The aggregated convection closer to TC center can decrease the RMW and then increase the IR. Therefore, a comprehensive account of the factors affecting convection distribution and RMW is crucial for characterizing TC IRs.

1.2 Tropical cyclone genesis

The genesis of TC still remains unknwon. Much research focuses on the genesis processes that can improve forecast skills and implement disaster prevention earlier. For researching each genesis process, previous studies classify different TC genesis types which will be discussed later. Also, TCs in different genesis types have different convection distribution (Ritchie and Holland 1999; Lee et al. 2008, 2010; Teng et al.

4
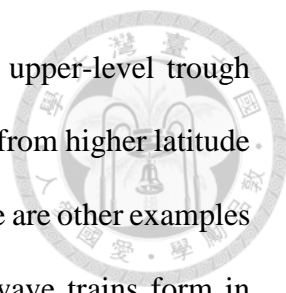
2020). Therefore, it is important to clarify the reasons and methods of previous studies classifying TC genesis types.

1.2.1 TC genesis processes

Previous studies have shown that TC genesis process is influenced by many factors in different scale. For the convection scale, active mesoscale convective systems (MCSs) and vertical hot towers (VHTs) can increase the vorticity through the mesoscale convective vortexes (MCVs) development and the latent heat release in convective cells (Hendricks et al. 2004; Houze et al. 2009). In addition, the convective self-aggregation driven by radiative feedback has been observed in the radiative-convective equilibrium (RCE) framworks (Wing et al. 2016; Muller and Romps 2018; Sobel et al. 2021; Tomassini 2021). In their RCE simulations, cyclogenesis can happen in synoptic scale without any background flow. Thus, convection may trigger a cyclonic circulation in synoptic-scale.

However, different synoptic-scale flow also affects the genesis processes through different convection distribution (Lee et al. 2008), and synoptic flow always happen in the real world rather then the idealized RCE simulation. Also, the interaction of synoptic flow and synoptic wave increase the vorticity in synoptic scale. For example, Chen et al. (2008) demonstrates that the easterly waves (EWs) enhance the monsoon trough circulations that favor TC genesis. In their study, midlatitude trough sometimes triggers the formation of monsoonal circulation. Furthermore, the tropical upper-tropospheric trough cells (TUTT-cells) not only affects the intensity (Chen and Wu 2023), but also influence the genesis of TC. Chen et al. (2008) imply that the TUTT-cells, also called "easterly wave–like disturbances", prompt the genesis process in rare cases (1.9%).

5
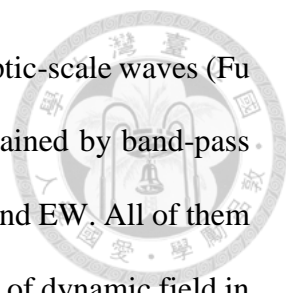
Moreover, a serie of research combine the TUTT and midlatittude upper-level trough effects (McTaggart-Cowan et al. 2008, 2013), suggesting that effects from higher latitude and upper level trough sometimes influence the genesis process. There are other examples of synoptic wave that favor TC genesis in tropical region. Some wave trains form in summer mean flow in the Western North Pacific (WNP) according to a serie of previous studies using band-pass filter (Fu et al. 2007; Xu et al. 2013). These wave trains include the Tropical Cyclone Energy Dispersion (TCED) and Synoptic Wave Train (SWT). In consequence, TC genesis can be induced by many synoptic systems.
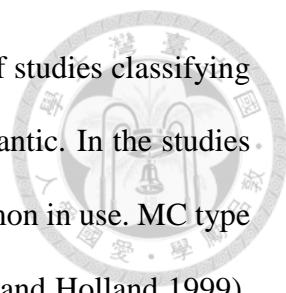
Furthermore, large-scale circulation plays an important rule in the frequency of TC genesis. Previous studies demonstrate some effects of quasi-biweekly oscillation (QBW), intraseasonal oscillation (ISO) and El Niño/Southern Oscillation (ENSO) (Fu et al. 2007; Xu et al. 2013; Li and Yu 2020; Dao and Yu 2021). For the low-frequency waves, QBW and ISO enhance the convection and positive vorticity, providing a favorable environment for genesis. Also, this low-frequency vorticity mostly contributes to monsoon-related environment, and affect the genesis process in different way (Hsieh et al. 2017). Teng et al. (2020) show that genesis in monsoon-related environment have more interaction angular momentum flux from the long-term scale at lower level. In summary, TC genesis is influenced by multiscale process, such as convection, synoptic-scale systems including synoptic waves and synoptic flow, and large-scale oscillations.

1.2.2 TC genesis types and their effects

In order to figure out several factors in the genesis processes, previous studies have done lots of work on classifying TC genesis types. TC genesis type is commonly classified based on either (i) synoptic-scale waves or (ii) environmental flow. As

6

doi:10.6342/NTU202303188

mentioned in section 1.2.1, a series of previous studies focus on synoptic-scale waves (Fu et al. 2007; Xu et al. 2013). They use synoptic-scale wind field obtained by band-pass filter and distinguish three kinds of TC genesis types: TCED, SWT, and EW. All of them are synoptic-scale waves. In their studies, they focus on the evolution of dynamic field in the genesis process, especially in synoptic scale. On the other hand, some researches classify genesis types by environmental flow (Lee et al. 2008; Teng et al. 2020). Lee et al. (2008) classify 6 genesis types by some critirias of wind speed around TC center: EW, northeasterly flow (NE), northeasterly and southwesterly flow (NE-SW), southwesterly flow (SW), monsoon confluence (MC), and monsoon sheer (MS). Teng et al. (2020) classify 5 genesis types by the K-means clustering algorithm (MacQueen 1967): easterly, monsoon confluence, southeast of monsoon trough, north of monsoon trough, and the monsoon trough. Based on the composite analysis in their studies conducted at the genesis time, each genesis type exhibits distinct structural characteristics, and extensive descriptions of their structures are provided. The definition of genesis time is commonly referred to the first time when TC intensity reaching 25 knots (Ritchie and Holland 1999; Lee et al. 2008; Teng et al. 2020). There are also a serie of researches that classify TC genesis types including synoptic-scale waves and environmental flow (Ritchie and Holland 1999; Yoshida and Ishikawa 2013; Fudeyasu and Yoshida 2018). Ritchie and Holland (1999) classify 5 genesis types: EW, MC, MS, Monsoon Gyre (MG), and Energy Dispersion (ED). The ED is equivalent to both preexisting TC (PTC) in Yoshida and Ishikawa (2013) and the TCED. Yoshida and Ishikawa (2013) consider the same classification but develop an objective scheme for identifying these features, and this method has been applied to many research (Yoshida et al. 2014; Fudeyasu and Yoshida 2018, 2019; Zhao et al. 2021; Wu and Fang 2023).

7
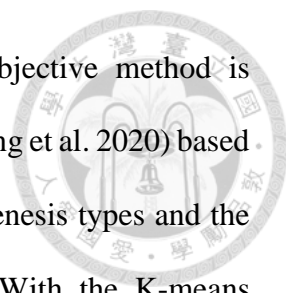
There are numerous classifications of TC genesis types. Most of studies classifying genesis types have the EW type, which is common in the North Atlantic. In the studies considering environmental flow, both of MC and MS types are common in use. MC type generally happen when the EW move into monsoon trough (Ritchie and Holland 1999), which is similar to the result of Chen et al. (2008). On the other hand, MS type forms inside the monsoon trough, which is similar to the composite of the monsoon tyough type in Teng et al. (2020). Previous studies classifying genesis types that include synoptic-scale waves always involve TCED. However, Ritchie and Holland (1999) have shown that TCED can develop in MC or MS environment, implying that TCED cases exactly overlap with other environmental flow types. Also, previous studies that use synoptic-scale waves to classify genesis types focus more on genesis processes rather than distinguish the structure of TC (Fu et al. 2007; Yoshida and Ishikawa 2013; Xu et al. 2013). In the numerical experiment, both SWT and EW have similar RMW contraction process (Ma and Li 2021), suggesting that the initial structural differences of genesis types in synoptic scale are quite small. Not only synoptic scale, but intraseasonal oscillations also affect the TC structure during TC genesis (Hsieh et al. 2017). Thus, synoptic-scale wave classification of TC genesis may fail to distinguish the TC structure since these processes usually occur simultaneously at different temporal scales. On the other hand, Lee et al. (2008) used environmental flow to classify genesis types and successfully find some convection features and flow patterns associated with genesis types, and these genesis types of environmental flow influence the outer size of TC (Lee et al. 2010). For example, the EW type has aggregated convection and the MCS near center, resulting in a small size when it become the tropical storm (TS). Also, this convection distribution can affect the inner-core dynamic of TC. However, their criterias

for classifying genesis types are based on subjective method. Thus, conducting an objective method is needed.

Furthermore, Joint Typhoon Warning Center (JTWC) defines another possible genesis type, monsoon depression, which is characterized by pressure field, such as the radius of outermost closed isobar (ROCI), and convection distribution (Lander and Guard 2001). Although the method of JTWC is too subjective and not quantified, it provides another environmental information. As shown in Figure 1.1, the composite wind field of monsoon depression defined by the JTWC at genesis time shows larger circulation than other TCs. Also, the composite moisture field demonstrates a wider distribution of moisture (Fig. 1.2), implying that this genesis type has unique structure and convection distribution, which can affect the inner-core dynamic of TC. Therefore, an objective classification of TC genesis based on environmental conditions, including wind, pressure and moisture fields, considers whole factors rather than focusing on only one scale.

1.3 Motivations and the scientific objectives

Previous studies have shown a negative correlation between the RMW and IR. The different convection distribution in each TC genesis type has been found. However, there is no study indentifying the specific impacts of TC genesis types on their inner-core structure, especially using objective method to classify each genesis type by several environmental conditions, such as flow pattern, pressure and moisture field. Moreover, many genesis types of environmental flow, namely the EW, MC, MS, have been dicussed for years. Many features of these genesis types have been discribed. It is notable to investigate how these features are found and divided into different genesis types in previous studies. Thus, the data distribution of these genesis types, such as the mean and

variance of atmospheric field, is important. In this study, an objective method is developed by the K-means clustering algorithm (MacQueen 1967; Teng et al. 2020) based on environmental conditions to examine the characteristics of TC genesis types and the connections with their inner-core structure, such as the RMW. With the K-means clustering, the distribution of some atmospheric parameters can be explicitly shown as the critical features are clustered in this framework. In order to understand the role of RMW and convection in different TC genesis types, a numerical experiment with the Advanced Research and Forecasting model (WRF) is conducted in a quasi-idealized experiment framework as developed in Chen and Wu (2023). The data and methodology are described in the Section 2. The Section 3 contains 2 parts, including the statistical analysis results of IR and each TC genesis type. The result of numerical experiment is demonstrated in the Section 4. Summary, discussion, and future works are described in the Section 5.

Chapter 2
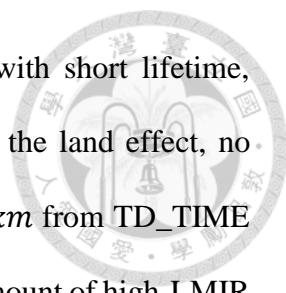
Data and Methodology

2.1 IBTrACS data

The International Best Track Archive for Climate Stewardship (IBTrACS) database is used in this study, containing the JTWC best track data. TC information in the WNP including location, intensity, and RMW are from the JTWC best track in the IBTrACS. Only cases reaching the intensity of TS (35 knots) are considered. In order to perform the most suitable environment for TC intensifying and prevent considering unfavorable environment, the lifetime maximum intensification rate (LMIR) is estimated. The beginning time of LMIR, reaching TS, and reaching 25 knots (genesis) is selected for analysis (i.e., I_TIME, TS_TIME, and TD_TIME). In total, 376 cases from 2006-2021 in the domain ($100°E-180°$, $0°-30°N$) at TD_TIME are selected. Also, the storm status evaluated by the JTWC, which provides information on whether it is classified as a monsoon depression, is included in the IBTrACS database. If cases are classified as monsoon depression once, they will be considered as the JTWC monsoon depression cases. There are 11 JTWC monsoon depression cases from the Sep. 2015 to Aug. 2020, and their composite fields are shown in Figure 1.1 & 1.2.

For the LMIR analysis, idealized cases (n=186) are selected. Thus, cases with favorable environment should be considered. First, according to previous studies, the 200-850 hPa VWS at I_TIME should be less than or equall to 8 ms^{-1} (Wang et al. 2015; Rios-Berrios and Torn 2017). The calculation of VWS will be discussed later. Second, to exclude the cases form at high latitude and suddenly experience the extratropical transition, the latitude at TS_TIME should be less than or equall to $26°N$ (Lee et al. 2008).

Third, to exclude the cases form in the South China Sea (SCS) with short lifetime, longitude at TS_TIME should be east of 121°*E*. Forth, to exclude the land effect, no landfall during LMIR period, and distance to land greater than 200 *km* from TD_TIME to LMIR period. The moisture field is not considered due to a large amount of high-LMIR cases in the dry environment although many low-LMIR cases in this similar moisture field. This implies that moisture affects the IR but its impact is not evident. To sum up, TCs in the favorable environment can be included in the LMIR analysis. With most of TCs in favorable environment and excluding the negative effects of environment, the influence of inner-core dynamic can be exhibited clearly. Therefore, RMW at I_TIME and TS_TIME is collected for LMIR analysis (i.e., I_RMW, TS_RMW).

2.2 ERA5 data

The ECMWF Reanalysis v5 (ERA5) data is used for the composite analysis of LMIR and TC genesis types to investigate the effect of genesis types on RMW and IR, including the composite of the JTWC monsoon depression cases (Fig. 1.1 and Fig. 1.2). In addition, to calculate the VWS, the ERA5 data is also utilized. Referenced from previous studies, the VWS is computed as the difference between wind speeds at 200 hPa and 850 hPa, averaged over an annular region ranging from 200 to 600 km away from TC center (DeMaria et al. 2005; Rogers et al. 2017; Lin et al. 2021). Unlike previous studies that used an annular region ranging from 200 to 800 km, the chosen range of 200-600 km in this study aims to encompass more cases with high-LMIR in the WNP. Also, ERA5 is also applied for classifying TC genesis types, including the computation of ROCI, which
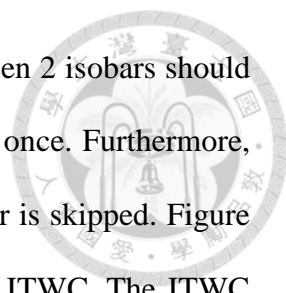
will be discussed later. However, the resolution of the ERA5 cannot detail the role of convection, suggesting that the numerical simulation is needed. Thus, TC field of the ERA5 at TD_TIME and 10-years monthly average of the ERA5 are selected for the initial TC field and background field in numerical simulation, respectively.
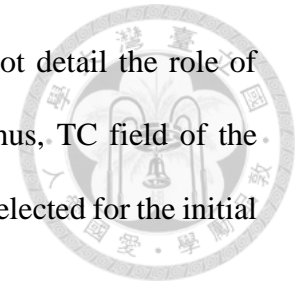
2.2.1 ROCI
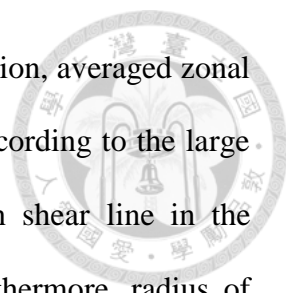
Because the method JTWC defining the monsoon depression include the moisture field and pressure field, it is valuable to include the information of moisture and pressure field in the new method of classifying TC genesis types. In this study, the ROCI at TD_TIME is selected for classifying TC genesis types, which is also used in the classification of monsoon depression in the JTWC. However, there are many small-scale eddies and the land effects in the ERA5 surface field that differ from those depicted on weather charts by meteorological agencies. Therefore, the 850 hPa geopotential height field is an alternative solution in this study. The method of finding the ROCI is used in Weber et al. (2014) that use data from the North Atlantic and Northeast Pacific basins. However, some steps are adjusted for 850 hPa geopotential height field of the ERA5 in the WNP. First, for finding TC center, the location of minimum geopotential height is choosed within $4° \times 4°$ box around the JTWC center instead of 500 km radius. Second, the number of radial legs for finding the pressure of outermost closed isobar (POCI) is 720 instead of 576, and the radius of radial legs is 14 degree with 0.2-degree resolution instead of 1500 km with 0.5 km resolution. Third, to prevent the effect of small-scale eddies, the interval of "isobar" is selected as 8 gpm instead of 1 hPa, and the smoothing of geopotential height within surounding 5 radial grid points is added. In addition, to

avoid the influence of another TC or disturbance, the distance between 2 isobars should be less than 5 degree. Also, a radial leg should cross an isobar only once. Furthermore, the process calculating geometrical centre of innermost closed isobar is skipped. Figure 2.1 shows the distribution of the ROCI evaluated by the ERA5 and JTWC. The JTWC have evaluated the ROCI at TD_TIME for 357 cases. The ROCI evaluated by JTWC is mostly concentrated between 200km and 400km, while the ROCI evaluated in this study is more dispersed, which is similar to previous study (Weber et al. 2014). The mean absolute difference and are 131.9535, which is similar to Weber et al. (2014) using data in another basins. The bias is 52.6821, larger than previous study that use data in another basins. However, the bias is still smaller than the other methods in previous study.

2.2.2 Classifying TC genesis types

Previous studies have shown different flow pattern with subjective mothods (Ritchie and Holland 1999; Lander and Guard 2001; Lee et al. 2008). In this study, several features that previous studies focus on are selected to perform an objective comparison between different genesis types. With an objective method that using several features from previous studies, the features of each genesis types can be well captured according to the data distribution and they can be compared to previous studies. Thus, ECMWF Reanalysis v5 (ERA5) environmental parameters are selected at 850hPa and the TD_TIME, as highlighted by previous studies, to perform a K-means cluster analysis for classifying TC genesis types (Fig. 2.2). First of all, averaged zonal wind in $5° \times 5°$ SW quadrant (u_SW) and averaged zonal wind in $5° \times 5°$ SE quadrant (u_SE) are selected according to the previous study that establish the critiria in these 2 areas to classify the

easterly and monsoon-related environment (Lee et al. 2008). In addition, averaged zonal wind in $5° \times 5°$ domain east of SE quadrant (u_ESE) is selected according to the large difference between the monsoon confluence region and monsoon shear line in the previous study (Ritchie and Holland 1999, see their Fig. 9). Furthermore, radius of outermost closed isobar (ROCI) is selected according to the definition of monsoon depression considered by the JTWC (Lander and Guard 2001). Also, averaged specific humidity in 5°-square domain around the center (q_inner) and averaged specific humidity in 10° hollow-square domain excluding the q_inner within the center (q_outer) are selected according to the definition of monsoon depression that include the "lack of persistent central convection" and "loosely organized cluster of MCS" by the JTWC (Lander and Guard 2001).

In this study, the Classifiability Index (CI) (Michelangeli et al. 1995) and the F1-score are used to determine the number of clusters in K-means clustering algorithm (Fig. 2.2). The F1-score considers the results of K-means clustering algorithm for different numbers of clusters and compares them with the cases evaluated as monsoon depressions by the JTWC in the IBTrACS database. Figure 2.3 shows the CI number indicates two peaks, one at 4 clusters and the other at 6 clusters. In addition, the F1-score shows the value of 4 clusters is higher than 6 clusters, implying that a genesis type in the result of 4 clusters is more similar to the definition of JTWC and provide an explainable result in this study. Hence, 4 clusters, such as 4 genesis types, are discussed. Due to the influence of "initial seeds" in the K-means algorithm (Michelangeli et al. 1995), the most common result of 100 iterations is selected in this study.

2.3 GPM_MERGIR data

NCEP/CPC L3 Half Hourly 4km Global Merged IR V1 (GPM_MERGIR) is used to provide the information of convection distribution in each TC genesis type. Similar to the ERA5, the GPM_MERGIR is selected for the composite field of each genesis type. In addition, GPM_MERGIR provides the brightness temperature (Tb) of cloud-top in higher resolution than the ERA5. Due to the missing value in the GPM_MERGIR, the calculation of composite excluding the missing value and averaging all the available grid points.

2.4 Numerical experiment settings

In order to estimate the effect of TC genesis types on intensification rate, a numerical experiment with WRF model 4.1.1 is conducted. In this study, two cases are chosen as initial vortexes based on the median RMW and the lowest Mean Square Deviation (MSD) of 850 hPa specific humidity composite field of two TC genesis types which will be discussed later. In addition, the vorticity inversion method developed in Wu et al. (2003) is used to generate dynamic field (u', v', ϕ') of these two cases from the ERA5 data. Furthermore, a quasi-idealized experiment framework developed in Chen and Wu (2023) is used to combine the dynamic field, thermodynamic field (T', RH') of TC (Fig. 2.4), and the 10-year climatological background field in August from the ERA5 (Fig. 2.5). Under this framework, the TC field is blended into the background field by using weighting average at 300-1000 km from the center. All the terrain is removed. Also, the sea surface temperature (SST) is fixed at 29℃. In WRF simulation, several parameters are selected, such as 6-day integration, vortex-following and two-way interactive triple-nested domain

with 9, 3, 1 km resolution. The Morrison microphysics, Mellor-Yamada-Janjic TKE scheme, RRTMG scheme, Kain-Fritsch (new Eta) scheme (9 km domain only) are used for microphysics, boundary layer, radiation, cumulus parameterization schemes, respectively.
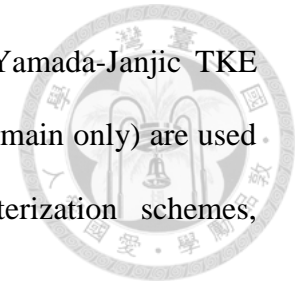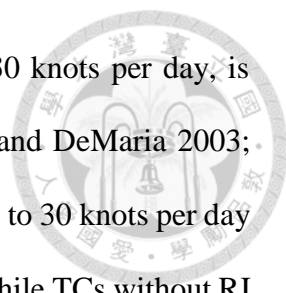
Chapter 3

Results --- Data analysis

3.1 Lifetime maximum intensification rate

3.1.1 TC inner-core dynamic factors

In order to estimate the effect of RMW on the intensification rate budget, as shown in Eq. 1-2, the LMIR, I_RMW, and TS_RMW in each case are calculated. Thus, the Eq. 1-2 can change to the explicit form:

$$\text{IR} = -\overline{u_m}\left(\frac{\overline{V_m}}{RMW} + \overline{f_m}\right) - \overline{w_m}\frac{\partial\overline{V_m}}{\partial z} + \overline{F_m} \quad (3\text{-}1)$$
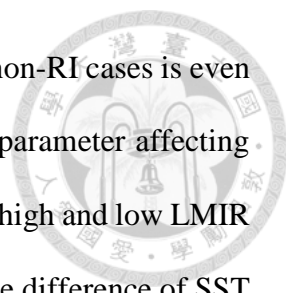
where the IR can be nearly to the LMIR if the RMW in right-hand side is the I_RMW. Figure 3.1 shows the negative correlation between LMIR and RMW in idealized cases, implying a nearly inverse proportion between the two in the LMIR period, which is consistent with the tangential wind tendency equation (Eq. 3-1). The smaller I_RMW implies larger curvature vorticity, which cause the stronger radial vorticity flux term in the Eq. 3-1 if radial inflow, intensity, and latitude stays the same, vise versia. TCs with larger I_RMW have lower LMIR due to weaker radial vorticity flux at the RMW, while others with smaller I_RMW have higher LMIR due to stronger radial vorticity flux at the RMW (Fig. 3.1a). Although the regression line referenced from the Eq. 3-1 shows a clear negative correlation, there still exists a certain amount of variance. The variance in each case may cause from different radial inflow, intensity, latitude, eddy and vertical advection term.

18

In addition, the common RI criteria, greater than or equal to 30 knots per day, is chosen to compare the features of TCs in different LMIR (Kaplan and DeMaria 2003; Carrasco et al. 2014). Overall, TCs with a LMIR greater than or equal to 30 knots per day have stronger RMW contraction in the past day ($\mu=17.5$ km day^{-1}), while TCs without RI have weaker RMW contraction in the past day ($\mu=7.08$ km day^{-1}), implying that stronger RMW contraction is associated with smaller I_RMW and higher LMIR. Also, this phenomenon appears in the difference between TS_RMW and I_RMW (Fig. 3.1b). The TCs with LMIR greater than or equal to 30 knots per day have similar TS_RMW around 50 to 100 km. However, their RMW contract to mostly below 50 km, which is shown in I_RMW. Hence, this evident RMW contraction cause a nearly inverse proportion between LMIR and I_RMW in all cases, which is clearer than TS_RMW. Moreover, TCs with larger TS_RMW usually have lower LMIR (< 30 knots per day) and do not experient the RI process (Fig. 3.1b), implying that the initial RMW can also affect LMIR. If TCs with larger TS_RMW have weaker RMW contraction, they will also have larger I_RMW and result in lower LMIR due to weaker radial vorticity flux at the large RMW which will be further validated in section. Therefore, the reason of large TS_RMW needs to be examined.

3.1.2 Environmental factors

Although the idealized cases are selected by excluding those with high VWS, nearness to land, and at high latitudes, the LMIR can still be affected by SST or dry air (DeMaria et al. 2005; Wang et al. 2021). Figure 3.2 shows pre-TC SST obtained at TD_TIME around the TC location of I_TIME, divided by different LMIR criteria. When the criteria is set at the common RI threshold (30 knots per day), there is no difference
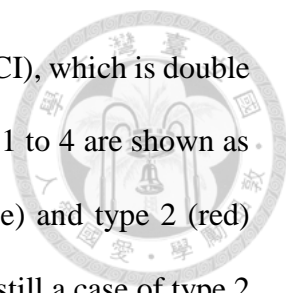
between the RI and non-RI cases (Figs. 3.2a, b). Instead, the SST of non-RI cases is even higher than that of RI cases, implying that the SST is not a critical parameter affecting the onset of RI process universally. However, the difference between high and low LMIR starts to appear when the LMIR criteria is set to 40 knots per day. The difference of SST composite is around 0.2℃ when the LMIR criteria is set to 50 or 60 knots per day. A possible reason is that the atmospheric conditions are more crucial for the RI onset than SST, but the SST enhance convection and radial vorticity flux, thus enhance the intensification rate when atmospheric conditions trigger the onset of RI process. If the atmospheric conditions inhibit the RI onset, they will not provide a favorable environment for deep convection around the TC center which can be enhanced by SST.

Among the different atmospheric conditions, RH affects the distribution of deep convection (Knaff et al. 2005). Figure 3.3 shows the 500 hPa RH around the TC location of I_TIME. There is a big difference around 10% in each LMIR criteria, while the 700 hPa RH has no difference (not shown). Overall, the higher LMIR cases have the higher RH around the center. When the criteria is set to 30 knots per day, there is another difference at the outer region, especially around -5° south of the center. In this region, the composite of non-RI cases has 5% higher RH than that of RI cases, which may be due to monsoonal flow that brings higher moisture from the Indian Ocean to south of the TC's center, and it will be dicussed in the Sesson 3.2.5.

3.2 TC genesis types
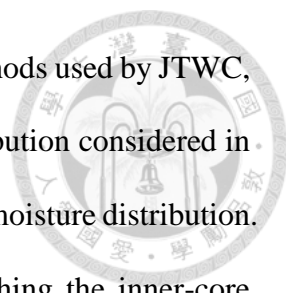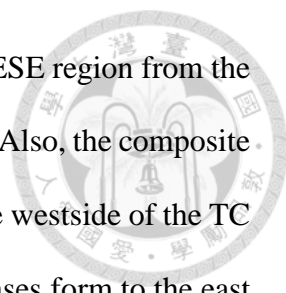
3.2.1 Composite of low-level structure

The distribution of the diameter of outermost closed isobar (DOCI), which is double of the ROCI, and u_ESE are shown in Figure 3.4. The genesis types 1 to 4 are shown as purple, red, green, and blue, respectively. First of all, type 1 (purple) and type 2 (red) overlap, but type 2 has smaller DOCI and u_ESE. However, there is still a case of type 2 with large u_ESE: Omeka (2010), which is an extratropical cyclone at $30°N$ and experience tropical transition outside the WNP (not shown). On the other hand, type 3 (green) and type 4 (blue) are characterized by larger u_ESE values, but type 4 has the largest DOCI. According to Figure 3.4, the u_ESE of type 1 is close to 0, implying that the westerly zonal wind ceases in the ESE area, which is similar to the composite of the monsoon confluence in the previous study (Ritchie and Holland 1999, see their Fig. 9). Therefore, type 1 is named as monsoon confluence (MC). Otherwise, the u_ESE of type 3 is stronger than type 1 with similar DOCI distribution, similar to the composite of the monsoon sheer in the previous study (Ritchie and Holland 1999, see their Fig. 9). Thus, type 3 is named as monsoon shear (MS). After analysis, most of cases in type 2 are associated with easterly waves. 1 case in type 2, Maria (2006), forms north of monsoon trough, with westerly flow located around -10° south of the center, but without evident westerly flow near south of the center (not shown). Therefore, type 2 is named as easterly wave (EW). After comparing with JTWC monsoon depression cases, which are from Sep. 2015 to Aug. 2020, it is found that type 4 cases overlap with JTWC monsoon depression cases. The F1-score between the two is 0.5, while the recall is 1, indicating that type 4 cases include all JTWC monsoon depression cases. This suggests that type 4 is the closest to monsoon depression. Thus, type 4 is named as monsoon depression (MD).

Apart from the overlapping cases between the MD cases and JTWC monsoon depression cases, there are still 22 cases that are not classified as JTWC monsoon

depression cases. A possible reason is the different classification methods used by JTWC, which considers convective distribution, varied from moisture distribution considered in this study. There might be some differences between convection and moisture distribution. However, considering the moisture plays a vital role in distinguishing the inner-core structure. In this study, MD cases are classified by stronger wind speed (u_ESE, u_SE, u_SW) and more moisture (q_inner, q_outer) by K-means algorithm (Fig. 3.4). The composites of MD cases show a larger circulation and wider moisture distribution (Fig. 3.5) similar to JTWC monsoon depression cases. Furthermore, although some JTWC monsoon depression cases have DOCI values around 500 km while the definition requires "on the order of 1000 km", MD cases in this study still include special cases with small DOCI or concentrated moisture distribution (Fig. 3.4). This could be due to MD cases also displaying other features in u_SW, u_SE, or u_ESE, and these special cases with similar zonal wind characteristics to other MD cases are grouped together in the same cluster by the K-means algorithm. Also, another possible factor is the uncertainty of subjective evaluation from the JTWC. Although the MD cases include 3 times more than the JTWC monsoon depression cases, the composite fields of them are similar (Fig. 1.1 and Fig. 3.5). Thus, it is worthy to analysis this type and compare with other types. To sum up, the K-means cluster analysis reveals four TC genesis types as illustrated in the 850hPa wind field referenced from previous studies: (i) monsoon confluence (MC), (ii) easterly wave (EW), (iii) monsoon shear (MS), and (iv) monsoon depression (MD).

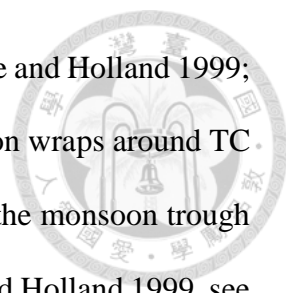TC genesis of MC type occurs southwest of the subtropical high (Fig. 3.5a). Moderate westerly flow exceeding 4 ms^{-1} is located to the southwest of the center, and easterly wind is located at the eastside of the center. This flow pattern is similar to monsoon confluence in previous studies (Ritchie and Holland 1999; Teng et al. 2020). After TC genesis at the confluence region where the westerly at the western side and

easterly at the eastern side, the westerly zonal wind extends into the ESE region from the western side of TC center when the TC circulation becomes stronger. Also, the composite of MC shows a clear open circulation with an open area located to the westside of the TC center, which can be interpreted as a monsoon trough, and the MC cases form to the east of the monsoon trough (Ritchie and Holland 1999, see their Figs. 8 and 9). According to the 850hPa vorticity field, a positive vorticity area indicates a monsoon trough either (Fig. 3.6a). The center of MC type is located to the east of a big positive vorticity area as the cases of MC type form to the east of the monsoon trough.

TC genesis of EW type occurs to the south of subtropical high, and within an easterly-dominating environment (Fig. 3.5b). No evident westerly flow occurs in the composite field, similar to easterly wave/easterly flow in previous studies (Ritchie and Holland 1999; Teng et al. 2020). Although a case of EW form at north of monsoon trough, there is still no evident westerly flow near south of the center in the composite. As many EW cases form and intensify in an easterly flow environment, the easterly flow located to south of TC center ceases and turns to weak westerly flow. Thus, the composite shows weak westerly flow lower than 4 ms^{-1} at south of TC center. In the 850hPa vorticity field, EW type has a small circulation and a small high positive vorticity area (Fig. 3.6b). According to the definition of vorticity, RMW locates inside the maximum of vorticity gradient as tangential wind drops outside the RMW causing a decay in curvature vorticity and negative shear vorticity. Thus, a small high positive vorticity area of the EW type implies a small RMW.

TC genesis of MS type occurs to the north of the westerly flow and to the south of the easterly flow (Fig. 3.5c). The westerly flow extends to the southeast of the center over the ESE region, and a strong wind core exceeding 12 ms^{-1} locates at south of the center,

23

similar to monsoon shear/monsoon trough in previous studies (Ritchie and Holland 1999; Teng et al. 2020). In the composite of MS type, a V-shaped circulation wraps around TC center with the opening to the west and the tip to the east, implying the monsoon trough clearly, and the MS cases form inside the monsoon trough (Ritchie and Holland 1999, see their Figs. 4 and 5). Similar to the MC type, the positive vorticity area indicates the presence of the monsoon trough in the 850hPa vorticity field of the MS type. The positive vorticity area extends from TC center to the west and east, also implying that the cases of MS type form inside the monsoon trough. Furthermore, the subtropical high in the composite of MS type is smaller than that in other types. One possible reason is that the location of subtropical high is distinct in the cases of MS type, resulting in a smooth and weak high-pressure area in the composite.

When TC genesis of MD type occurs, there is a characteristically larger circulation (Fig. 3.5d), and the wind field exceeding $4ms^{-1}$ extends to 10° away from the center, similar to the composite of MD cases in JTWC best track (Fig. 1.1). Similar to the MS type, the westerly flow of MD type is evident but stronger, which exceeds 14 ms^{-1}. Furthermore, the whole circulation of MD type is 2 ms^{-1} stronger than the MS type. Also, MD type has a large circulation and a large high positive vorticity area which implies a larger RMW according to the definition of vorticity (Fig. 3.6d). A possible reason is that the monsoon trough has become a monsoon depression with a circular circulation (Beattie and Elsberry 2012), and turns into the MD type TC. As a result, the large circular circulation and high positive vorticity area observed in the MD type composite are attributed to the transformation of the monsoon trough into a monsoon depression with big circulation.
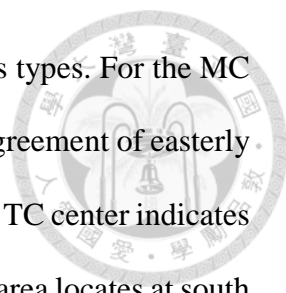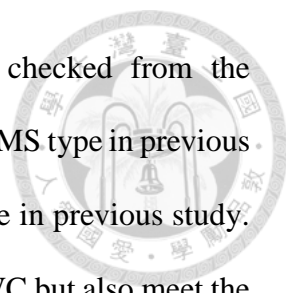
Figure 3.17 shows the variance of wind field in different genesis types. For the MC type, low variance area locates at east of TC center indicates a high agreement of easterly at the east. For the EW type, low variance area locates at southwest of TC center indicates a high consensus of very weak westly. For the MS type, low variance area locates at south of TC center indicates a high agreement of westerly at the south. The different sizes within the MD cases result in higher variance compared to other types. Also, there is a high variance area locates at west of the domain in the MC, MS and MD types, implying that these 3 types also include the PTC cases in previous studies due to the occurrence of previous TCs raising the variance. In the variance of moisture distribution in MD type, there is a large low variance area (Fig. 3.18d), implying that MD cases are classified due to the large moist area which will be dicussed later.

In this study, the examination of subjective method from the classic previous study is conducted (Ritchie and Holland 1999). In addition, the comparison of MD definition in this study and the JTWC is implemented (Lander and Guard 2001). The comparison of subjective and objective method is shown in Table 3.1. The objective method presents a higher number of MC cases. However, 18.9% of these MC cases may be classified into MS type in the previous study. Lots of them genesis in a northwest-southeast orientation confluence region/shear line. They concurrently meet the conditions of easterly wind at the eastern side and westerly wind at the southern side. Therefore, distinguishing the genesis type of these cases is difficult due to this continuous monsoonal flow pattern. Also, some cases form at the Inter-Tropical Convergence Zone (ITCZ) with strong easterly at the north but weak westerly at the south during winter time, and these cases result in a higher percentage of the MC type during winter time (Fig. 3.14b). Thus, these MC cases in this study may be classified as MS type in previous studies due to wide but weak westerly wind in the south. In addition, some of MD cases in this study do not meet

25

the definition of the JTWC due to the convection distribution checked from the GPM_MERGIR data. Among these cases, 13 cases are classified into MS type in previous study, suggesting that some MD cases are still similar to the MS type in previous study. Furthermore, all 65 MD cases not only meet the definition of the JTWC but also meet the definition of the MS type in the previous study. However, wind field and the other parameters show the different structure (Fig. 3.5). Also, the MD type is similar to the MG type in previous study either based on a large DOCI definition, but the discussion of MG type in previous study focus on their "confluence region". Thus, the MG type in the previous study may be similar to both MD and MC types in this study, as it forms inside or east of a large circulation.

Compared to another previous study using an objective method either, the convection distribution from the inner core to the outer region shows an evident difference in each genesis type (Fig. 3.11), while the previous study showed a nearly similar distribution around the center (Fudeyasu and Yoshida 2018; see their Fig. 4), revealing that this new method can better classify their structure and inner-core dynamics.

3.2.2 Composite of upper-level structure

Figures 3.7 & 3.8 present the composite of the 200 hPa wind field and the 200-850 hPa VWS. Due to the influence of the South Asian High, both the MS and MD types experience stronger northeasterly winds at 200 hPa. Also, both types have stronger southwesterly wind in the southwest quadrant. This thermal wind within the monsoon system leads to a stronger VWS environment in the MS and MD types, especially in the southwest quadrant. Overall, the MD type experiences the strongest VWS, followed by the MS type. The VWS in the MS type is weaker, particularly around -20° north of the
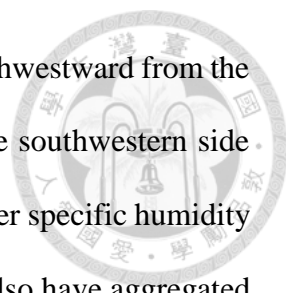
center. The possible reason is that the genesis location is farther south, resulting in a greater distance from the polar jet at the upper level. The EW type, on the other hand, encounters the weakest VWS because of the eastmost genesis location, which will be dicussed in the section 3.2.4.
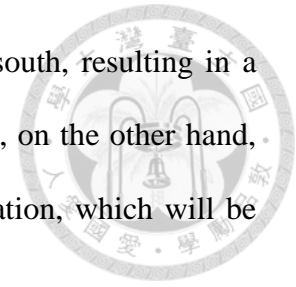
Chen et al. (2008) showed the "fake" easterly waves caused from the TUTT-cells, and they induced only 3% genesis cases much fewer than EW, which diracterly induced 25% genesis cases. Composite shows no cyclonic structure at 200 hPa, which means no evident TUTT-cells influence on each type although several cases form around the TUTT-cells (Fig. 3.9). Therefore, the influence of TUTT-cells or other upper-level troughs may exist but not evident in the WNP.

3.2.3 Convection statistics

Figure 3.10 & 3.11 show the composite of 850 hPa specific humidity and the Tb field of cloud-top. In the MD type, there is a large area of scattered convection with specific humidity exceeding 0.013 kg/kg (Figs. 3.10d and 3.11d), which can cause inflow in the outer region. Therefore, the large RMW in the MD cases forms due to a tangential wind increase through the radial vorticity flux in the outer area. In contrast, EW type has a higher specific humidity and lower Tb only around the center (Figs. 3.10b and 3.11b). In the EW type, the area where Tb is lower than 270K is only around 500km from the center, while that of the MD type is extend to over 1000km from the center. Also, the maximum of Tb is located at the center in the EW type composite. In contrast, the maximum of Tb is nearly 250km away from the center in the MD type composite.

Since the specific humidity distribution of MC type extends southwestward from the center (Fig. 3.10a), outer convection in those cases is usually on the southwestern side (Fig. 3.11a). Otherwise, MS type has an east-west orientation of higher specific humidity and lower Tb (Figs. 3.10c and 3.11c). However, MC and MS types also have aggregated convection and moisture around center similar to EW. On the other hand, the moisture of MD type is much wider than others. The Tb maximum of MS type is nearly 100km from the center, similar to the MD type. It may because the VWS of the MS and MD type is higher than EW and MC types, but the Tb maximum of MD is farther due to wider moisture distribution or higher VWS.

3.2.4 Track and seasonality

Figures 3.12 and 3.13 show the tracks and locations of the four genesis types. EW cases have more westward tracks than the others (Fig. 3.12b) because they usually form at the easternmost location of genesis (Fig. 3.13a), such as the south of the subtropical high with an easterly flow environment (Fig. 3.5b), and continue moving westward in this environment. On the other hand, MC cases usually form to the west of EW's genesis location (Fig. 3.13a), at the southwest of subtropical high where they can be easily driven northeastward by the upper-level trough at the westside of subtropical high (Fig. 3.5a). Thus, MC cases have more recurving tracks than EW (Fig. 3.12a).

However, MS and MD cases usually form inside the monsoon trough, which means many of them have a more western genesis location closer to land than MC and EW cases (Fig. 3.13a), resulting in irregular tracks due to the lack of steering flow in the monsoon

trough. Also, the influence of land may prohibit the intensification in MS or MD type, causing a lower LMIR.
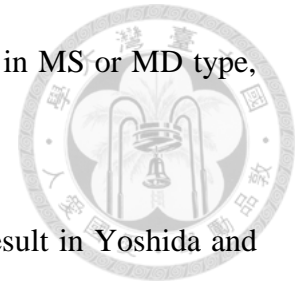
The seasonality is shown in Figure 3.14. Different from the result in Yoshida and Ishikawa (2013), the number of cases for EW and MC types peaks in September, while that for MS type peaks in August. Also, the percentage of MS type is higher during June to August (Fig. 3.14b), totally different from the result in Yoshida and Ishikawa (2013) showing lower percentage. A possible reason is that the MS type in this study is classified by stronger zonal wind at south of TC center, while the MS type in the previous study is defined by larger difference of zonal wind between the north and the south. Therefore, more MS cases are detected during winter in the previous study due to strong easterly at the north and moderate westerly caused by the ISO at the south. In this study, these cases with moderate westerly are usually classified as MC, also associate with weak u_ESE. According to the increased activity of MS and MD types in summer when the monsoon trough is evident, the seasonality of TC genesis types in this study is reasonable.

3.2.5 The effects on TC inner-core dynamic

The TS_RMW and LMIR are included in the IBTrACS, thus the relationship in the TS_RMW, LMIR, and TC genesis types are explicit in idealized cases when the mean and standard deviation are demonstrated in Figure 3.15. Owing to the larger circulation and more scattered convection, MD types have a significantly larger TS_RMW ($p = 0.000623$) and lower LMIR ($p = 0.000161$) than EW types according to Conover's

test (Fig. 3.16). By the analysis of variance (ANOVA), MD types also have a significantly larger TS_RMW $(p = 0.000409)$ and lower LMIR $(p = 0.000008)$ than EW types.

Although MC and MS types have intermediate TS_RMW between EW and MD types (Fig. 3.16a), MC and MS types have aggregated convection similar to EW (Fig. 3.11a and c), leading to radial inflow on the inner side of RMW. According to previous study (Wu and Ruan 2021), this inflow causes RMW contraction via radial fluxes of vorticity term, resulting in small I_RMW similar to EW. Finally, due to the radial fluxes of vorticity term of MC and MS types on the RMW, their LMIR is similar to that of EW. Therefore, MC and MS types have significantly higher LMIR than MD $(\text{MC: } p = 0.000230, \text{MS: } p = 0.000161)$ by the Conover's test and the ANOVA $(\text{MC: } p = 0.000052, \text{MS: } p = 0.000023)$ (Fig. 3.16b).

Chapter 4

Results --- Numerical experiment

4.1 Overview of the experiment results

Limitations of the IBTrACS and ERA5 analyses respectively include subjective evaluation from the weather forecast agency and the coarse resolution of reanalysis data. Due to these limitations, there is lack of information on the role of convection and tangential wind tendency. To address the above issue, quasi-idealized experiments are conducted to examine the role of convection and tangential wind tendency, thus better characterizing TC intensification rates. According to the largest difference in TS_RMW between EW and MD types (Fig. 3.16a), two cases: Utor (2013) and Omais (2016) are selected from these two types for simulations. The initial field shown in Figure 4.1 implies an evident initial RMW difference between EW and MD types.

Figure 4.2 shows the minimum sea-level pressure and maximum surface wind speed change of the EW and MD in the simulations. Due to the difference in initial intensity, the timing with similar intensity are selected for the later comparison, i.e., EW at 48 h and MD at 24 h. Comparing the following 72 h after these two reference times and calculating the moving average, the LMIR of EW and MD is 42.4 knots per day and 27.0 knots per day, respectively. The LMIR obtained from the numerical experiments is similar to that in the IBTrACS database (Fig. 3.15 and 3.16b), but the LMIR of numerical experiments is higher than the mean LMIR of these genesis types due to the quasi-idealized environment. However, the result of simulation is still similar to some cases of

these 2 types. For example, the cloud evolution of MD in simulation is smilar to the real case: Dujuan (2015), which is also a JTWC monsoon depression case.
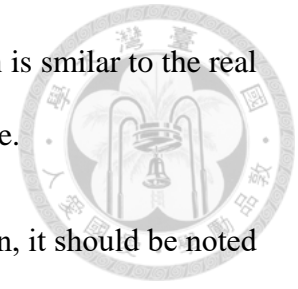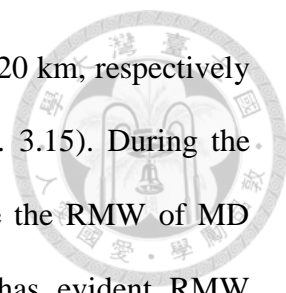
Although the ocean condition is suitable for TC's intensification, it should be noted that the atmospheric conditions can change when TC moves to different position due to the climatological boundary conditions. In the simulation, their environmental conditions are similar (Fig. 4.3). The VWS of EW and MD is lower than 8 ms^{-1} during most of the intensifying period (Figs. 4.3a, b). Although the RH is higher in MD experiment, which means more suitable for intensification, the LMIR of MD is lower than EW, implying that the difference in RH weakly affects the LMIR (Figs. 4.3c, d).

However, the VWS of MD increases to near 8 ms^{-1} at the 12 hr, coherent with the time when MD ceases to intensify. Therefore, checking the influence of VWS on TC structure in the MD experiment is needed. However, there is no significant upper-level shifting when VWS increases (Figs. 4.4b, d, f). Furthermore, the lower-level wind field and model-derived reflectivity shows MD with multiple centers and merging when MD ceases to intensify (Figs. 4.5b, d, f and Figs. 4.6b, d, f). Also, the VWS of EW is higher than MD while EW experiences higher IR later, implying that changes in the inner core structure have more effect on intensification than VWS during this period.

4.2 TC inner-core dynamic analysis

To investigate the role of RMW and inflow, an azimuthal-mean framework focusing on 500 m is conducted according to previous studies (Stern et al. 2015; Li et al. 2021). In general, the RMW contraction process and IR of EW and MD are different. The RMW

of EW and MD at the initial analyzed period is around 40 km and 120 km, respectively (Figs. 4.7a, b), which is similar to the result from IBTrACS (Fig. 3.15). During the intensification period, the RMW of EW contracts to 20 km, while the RMW of MD contracts to 40 km and then stops contracting. Although MD has evident RMW contraction than that in EW (Figs. 4.7c, d), the final RMW of MD is over twice as large as that of EW. On the other hand, EW has higher intensification rate than MD. When the RMW contractions reach its maximum, the intensification rates also reach its maximum, which is similar to the result from Stern et al. (2015). During the period when the RMW remains unchanged around the 36 h in EW and the 60 h in MD, EW still has a clear intensification rate, while MD does not intensify anymore.

Figure 4.8 shows the positive and negative contribution terms of the tangential wind tendency equation at the RMW, based on the method in Li et al. (2021). Overall, EW has larger value than MD. During the 12 to 24 h, the positive term of EW is 2000 ms^{-1} day^{-1} approximately, clearly larger than the negative term of EW, which is near 1500 ms^{-1} day^{-1} (Figs. 4.8 a, b). Although the positive term in MD increases later, the negative term also arises to the similar value because the surface friction and subgrid-scale diffusion term becomes larger when the intensity, such as wind speed, gets stronger. In addition, the positive term of the tangential wind tendency equation is associated with the radial fluxes of absolute vorticity, which contains radial wind and vorticity. The radial wind of EW and MD is similar at the 24 h (Figs. 4.8 c, d), but the vorticity of EW is surprisingly larger than that in MD. Although MD intensifies later, there is still a big difference in vorticity, implying that the difference in RMW strongly influences the vorticity field, thus resulting in the difference in radial fluxes of absolute vorticity, and intensification rate.
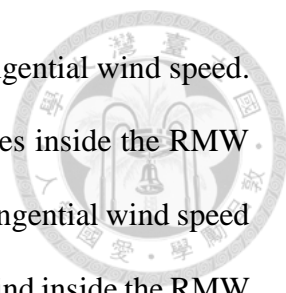
33

Figure 4.9 presents the Hovmöller diagram of change rate of tangential wind speed. The maximum increasing rate of tangential wind speed always locates inside the RMW in the MD experiment. In contrast, the maximum increasing rate of tangential wind speed locates at the RMW in the EW experiment. Although the tangential wind inside the RMW increase in the MD experiment, the RMW of MD is still smaller than EW. Also, the lower increasing rate at RMW implies the lower intensification rate than EW. It should be note that the RMW contraction cause smaller RMW. However, the final RMW of MD is larger than EW, causing weaker vorticity around the RMW (Fig. 4.10). Therefore, another factor prohibits the RMW contraction. According to previous studies (Stern et al. 2015; Li et al. 2021), the RMW contraction rate affected by the radial curvature of tangential wind. During the period of RMW contraction and intensification, which means that the tangential wind speed at RMW increases, the radial curvature of tangential wind around RMW also increases. The increasing of radial curvature around RMW indicates that the wind speed difference between RMW and its inner side increases, limiting the probability of wind speed inside RMW surpassing that at the RMW. Consequently, this difference stops the RMW contraction in MD at the 36 h. Also, this phenomenon is also shown in EW at the 24 h. Furthermore, the absence of convection inside the RMW also prohibits the inflow inside the RMW (Figs. 4.6e, f and Fig. 4.10), thus reduses the increasing rate of tangential wind speed inside the RMW (Fig. 4.9).

At the mature stage, MD has scattered convection whereas EW has aggregated convection (Fig. 4.11). This pattern is similar to that at the TD_TIME in the composite analysis of TC genesis types (Fig. 3.11). Due to the scattered convection of MD (Fig. 4.11b), the area of inflow extends widely instead of located around the RMW (Fig. 4.10b). With the much weaker vorticity at RMW, the inflow of MD is not strong enough to cancel the difference of vorticity, causing smaller positive contribution term in the tangential

34

wind tendency equation (Fig. 4.8a). Also, both MD and EW have a clear curved tangential wind profile, implying that the tangential wind inside the RMW have to increase significantly to surpass the tangential wind on the RMW and cause RMW contraction. Thus, this characteristic limit the RMW contraction of MD. On the other hand, EW has compact convection around the center and weak convection in the outer region (Fig. 4.11a), which is similar to the result in Peng and Wu (2020). The aggregated convection, smaller RMW and larger vorticity advection of EW result in a higher final intensity than MD.

Chapter 5

Conclusions

5.1 Summary and discussions

Previous studies have showed the process of RMW contraction and intensification, and a negative correlation between the RMW and IR is observed (Carrasco et al. 2014; Xu and Wang 2018a; Li et al. 2021; Wu and Ruan 2021). However, there is a knowledge gap in the correlation between TC genesis structure and RMW size while previous studies focus more on genesis process although many methods of classifying genesis types developed (Lee et al. 2008; Ritchie and Holland 1999; Teng et al. 2020; Yoshida and Ishikawa 2013). In this study, A new method is developed to classify TC genesis types based on environmental factors. This new method can distinguish different structures when TCs form. Hence, each genesis type in this study has a distinct RMW range and convection distribution, which could affect RMW contraction. In summary, TC genesis of MD type has a larger circulation and scattered convection, thus leading to larger RMW and lower LMIR based on tangential wind tendency equation, while EW, MC, and MS types have aggregated convection result in higher LMIR.

Furthermore, the quasi-idealized experiments are conducted to verify the effect of RMW and convection with high resolution WRF model. According to the tangential wind tendency equation, EW obtains a larger IR due to a smaller RMW and compact convection causing larger vorticity flux at the RMW, while MD has a larger RMW and scattered convection resulting in a smaller IR. Although the RMW of MD continues to contract and the IR increases, its LMIR is not as high as that of EW because its RMW is

still larger. As shown in the schematic diagram (Fig. 5.2), scattered convection of MD with scattered diabatic heating creates a widely tangential wind increase instead of focusing around the RMW, which prevents the higher IR although convection inside the RMW causes it to contract. In addition, the final RMW of MD is over twice as large as that of EW due to the curved tangential wind profile which prevents the RMW contraction during the mature stage. As a result, EW maintains a higher LMIR and final intensity due to its smaller RMW throughout the analyzed period than MD.

5.2 Future works

Based on the quasi-idealized environment of numerical experiment in this stidy, the influence of VWS is observed. The VWS can lead to asymmetrical convection distribution, resulting in the differences in vorticity and inflow, potentially affecting the RMW contraction and IR through non-axisymmetric vorticity flux terms. Thus, discussion about the effect of non-axisymmetric vorticity flux is needed. Also, the disturbances of EW and MD types are implanted into same background field in the numerical experiments of this study. For future work, different background fields should be considered since they genesis in different environments based on the composite analysis. Furthermore, the initial disturbances of MC and MS types is worth to be conducted in the numerical experiment. Although the TC intensity of initial field is 25kt in the IBTrACS, there are differences in intensity compared to ERA5 data. The wind field of MD is stronger than EW. It is worth exploring whether it is necessary to adjust the initial intensity to match the intensity from IBTrACS. Also, whether IBTrACS is closer to reality than the ERA5 is valuable to be discuss. Therefore, conducting more observations during TC genesis is necessary, to obtain more accurate initial wind fields
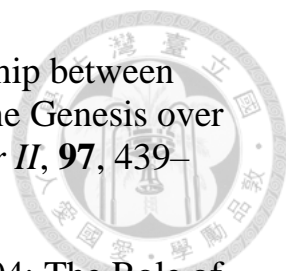
and further observe how moisture and convective distribution influence the initial RMW

of TC.

References
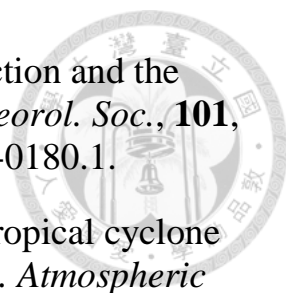
Beattie, J. C., and R. L. Elsberry, 2012: Western North Pacific monsoon depression formation. *Weather Forecast.*, **27**, 1413–1432, https://doi.org/10.1175/WAF-D-11-00094.1.

Carrasco, C. A., C. W. Landsea, and Y. L. Lin, 2014: The influence of tropical cyclone size on its intensification. *Weather Forecast.*, **29**, 582–590, https://doi.org/10.1175/WAF-D-13-00092.1.

Chen, T. C., S. Y. Wang, M. C. Yen, and A. J. Clark, 2008: Are tropical cyclones less effectively formed by easterly waves in the Western North pacific than in the North Atlantic? *Mon. Weather Rev.*, **136**, 4527–4540, https://doi.org/10.1175/2008MWR2149.1.

Chen, Y.-A., and C.-C. Wu, 2023: Environmental Forcing of Upper-Tropospheric Cold Low on Tropical Cyclone Intensity and Structural Change. *J. Atmospheric Sci.*, **80**, 1123–1144, https://doi.org/10.1175/JAS-D-22-0131.1.

Dao, L. T., and J.-Y. Yu, 2021: Impacts of Madden–Julian oscillation on tropical cyclone activity over the South China Sea: Observations versus HiRAM simulations. *Int. J. Climatol.*, **41**, 830–845, https://doi.org/10.1002/joc.6673.

DeMaria, M., M. Mainelli, L. K. Shay, J. A. Knaff, and J. Kaplan, 2005: Further Improvements to the Statistical Hurricane Intensity Prediction Scheme (SHIPS). *Weather Forecast.*, **20**, 531–543, https://doi.org/10.1175/WAF862.1.

Emanuel, K. A., 1988: The Maximum Intensity of Hurricanes. *J. Atmospheric Sci.*, **45**, 1143–1155, https://doi.org/10.1175/1520-0469(1988)045<1143:TMIOH>2.0.CO;2.

Fu, B., T. Li, M. S. Peng, and F. Weng, 2007: Analysis of tropical cyclogenesis in the Western North Pacific for 2000 and 2001. *Weather Forecast.*, **22**, 763–780, https://doi.org/10.1175/WAF1013.1.

Fudeyasu, H., and R. Yoshida, 2018: Western North Pacific tropical cyclone characteristics stratified by genesis environment. *Mon. Weather Rev.*, **146**, 435–446, https://doi.org/10.1175/MWR-D-17-0110.1.

——, and ——, 2019: Statistical Analysis of the Relationship between Upper Tropospheric Cold Lows and Tropical Cyclone Genesis over the Western North Pacific. *J. Meteorol. Soc. Jpn. Ser II*, **97**, 439–451, https://doi.org/10.2151/jmsj.2019-025.

Hendricks, E. A., M. T. Montgomery, and C. A. Davis, 2004: The Role of "Vortical" Hot Towers in the Formation of Tropical Cyclone Diana (1984). *J. Atmospheric Sci.*, **61**, 1209–1232, https://doi.org/10.1175/1520-0469(2004)061<1209:TROVHT>2.0.CO;2.

Houze, R. A., W. C. Lee, and M. M. Bell, 2009: Convective contribution to the genesis of Hurricane Ophelia (2005). *Mon. Weather Rev.*, **137**, 2778–2800, https://doi.org/10.1175/2009MWR2727.1.

Hsieh, Y. H., C. S. Lee, and C. H. Sui, 2017: A study on the influences of low-frequency vorticity on tropical cyclone formation in the western North Pacific. *Mon. Weather Rev.*, **145**, 4151–4169, https://doi.org/10.1175/MWR-D-17-0085.1.

Huang, Y. H., C. C. Wu, and M. T. Montgomery, 2018: Concentric eyewall formation in Typhoon Sinlaku (2008). Part III: Horizontal momentum budget analyses. *J. Atmospheric Sci.*, **75**, 3541–3563, https://doi.org/10.1175/JAS-D-18-0037.1.

Kaplan, J., and M. DeMaria, 2003: Large-Scale Characteristics of Rapidly Intensifying Tropical Cyclones in the North Atlantic Basin. *Weather Forecast.*, **18**, 1093–1108, https://doi.org/10.1175/1520-0434(2003)018<1093:LCORIT>2.0.CO;2.

Knaff, J. A., C. R. Sampson, and M. DeMaria, 2005: An Operational Statistical Typhoon Intensity Prediction Scheme for the Western North Pacific. *Weather Forecast.*, **20**, 688–699, https://doi.org/10.1175/WAF863.1.

Lander, M. A., and C. P. Guard, 2001: Western North Pacific, North Indian Ocean, and Southern Hemisphere Tropical Cyclones of 1997. *Mon. Weather Rev.*, **129**, 3015–3036, https://doi.org/10.1175/1520-0493(2001)129<3015:WNPNIO>2.0.CO;2.

Lee, C. S., K. K. W. Cheung, J. S. N. Hui, and R. L. Elsberry, 2008: Mesoscale features associated with tropical cyclone formations in the Western North Pacific. *Mon. Weather Rev.*, **136**, 2006–2022, https://doi.org/10.1175/2007MWR2267.1.

——, ——, W. T. Fang, and R. L. Elsberry, 2010: Initial maintenance of tropical cyclone size in the Western North Pacific. *Mon. Weather Rev.*, **138**, 3207–3223, https://doi.org/10.1175/2010MWR3023.1.

Li, T. H., and Y. Wang, 2021: The role of boundary layer dynamics in tropical cyclone intensification. Part ii: Sensitivity to initial vortex structure. *J. Meteorol. Soc. Jpn.*, **99**, 555–573, https://doi.org/10.2151/jmsj.2021-028.

Li, Y., Y. Wang, and Y. Lin, 2019: Revisiting the dynamics of eyewall contraction of tropical cyclones. *J. Atmospheric Sci.*, **76**, 3229–3245, https://doi.org/10.1175/JAS-D-19-0076.1.

——, ——, L. I. N. Yanluan, and A. X. I. N. Wang, 2021: Why does rapid contraction of the radius of maximum wind precede rapid intensification in tropical cyclones? *J. Atmospheric Sci.*, **78**, 3441–3453, https://doi.org/10.1175/JAS-D-21-0129.1.

Li, Y.-X., and J.-Y. Yu, 2020: Why rare tropical cyclone formation after maturity of super El Niño events in the western North Pacific? *Terr. Atmospheric Ocean. Sci.*, **31**, 21–32, https://doi.org/10.3319/TAO.2019.06.23.01.

Lin, I. I., and Coauthors, 2021: A tale of two rapidly intensifying supertyphoons: Hagibis (2019) and haiyan (2013). *Bull. Am. Meteorol. Soc.*, **102**, E1645–E1664, https://doi.org/10.1175/BAMS-D-20-0223.1.

Ma, C., and T. Li, 2021: Effects of perturbation type on tropical cyclone size over tropical North Western Pacific and Atlantic. *Clim. Dyn.*, **56**, 475–489, https://doi.org/10.1007/s00382-020-05488-9.

MacQueen, J., 1967: Some methods for classification and analysis of multivariate observations. *Proc Fifth Berkeley Symp. Math. Stat. Probab. 1967*, 281–297.

McTaggart-Cowan, R., G. D. Deane, L. F. Bosart, C. A. Davis, and T. J. Galarneau, 2008: Climatology of tropical cyclogenesis in the North Atlantic (1948-2004). *Mon. Weather Rev.*, **136**, 1284–1304, https://doi.org/10.1175/2007MWR2245.1.

——, T. J. Galarneau, L. F. Bosart, and R. W. Moore, A Global Climatology of Baroclinically Influenced Tropical Cyclogenesis*. https://doi.org/10.1175/MWR-D-12-00186.1.

Michelangeli, P.-A., R. Vautard, and B. Legras, 1995: Weather Regimes: Recurrence and Quasi Stationarity. *J. Atmospheric Sci.*, **52**, 1237–1256, https://doi.org/10.1175/1520-0469(1995)052<1237:WRRAQS>2.0.CO;2.

Muller, C. J., and D. M. Romps, 2018: Acceleration of tropical cyclogenesis by self-aggregation feedbacks. *Proc. Natl. Acad. Sci.*, **115**, 2930–2935, https://doi.org/10.1073/pnas.1719967115.

Peng, C. H., and C. C. Wu, 2020: The impact of outer-core surface heat fluxes on the convective activities and rapid intensification of tropical cyclones. *J. Atmospheric Sci.*, **77**, 3907–3927, https://doi.org/10.1175/JAS-D-19-0348.1.

Rios-Berrios, R., and R. D. Torn, 2017: Climatological Analysis of Tropical Cyclone Intensity Changes under Moderate Vertical Wind Shear. *Mon. Weather Rev.*, **145**, 1717–1738, https://doi.org/10.1175/MWR-D-16-0350.1.

Ritchie, E. A., and G. J. Holland, 1999: Large-Scale Patterns Associated with Tropical Cyclogenesis in the Western Pacific. *Mon. Weather Rev.*, **127**, 2027–2043, https://doi.org/10.1175/1520-0493(1999)127<2027:LSPAWT>2.0.CO;2.

Rogers, R. F., and Coauthors, 2017: Rewriting the Tropical Record Books: The Extraordinary Intensification of Hurricane Patricia (2015). *Bull. Am. Meteorol. Soc.*, **98**, 2091–2112, https://doi.org/10.1175/BAMS-D-16-0039.1.

Sobel, A. H., A. A. Wing, S. J. Camargo, C. M. Patricola, G. A. Vecchi, C. Y. Lee, and M. K. Tippett, 2021: Tropical Cyclone Frequency. *Earths Future*, **9**, https://doi.org/10.1029/2021EF002275.

Stern, D. P., J. L. Vigh, D. S. Nolan, and F. Zhang, 2015: Revisiting the relationship between eyewall contraction and intensification. *J. Atmospheric Sci.*, **72**, 1283–1306, https://doi.org/10.1175/JAS-D-14-0261.1.

Teng, H. F., J. M. Done, C. S. Lee, H. H. Hsu, and Y. H. Kuo, 2020: Large-scale environmental influences on tropical cyclone formation processes and development time. *J. Clim.*, **33**, 9763–9782, https://doi.org/10.1175/JCLI-D-19-0709.1.

Tomassini, L., 2021: The interaction between moist convection and the atmospheric circulation in the tropics. *Bull. Am. Meteorol. Soc.*, **101**, E1378–E1396, https://doi.org/10.1175/BAMS-D-19-0180.1.

Wang, Y., and C. C. Wu, 2004: Current understanding of tropical cyclone structure and intensity changes - A review. *Meteorol. Atmospheric Phys.*, **87**, 257–278, https://doi.org/10.1007/s00703-003-0055-6.

——, Y. Rao, Z.-M. Tan, and D. Schönemann, 2015: A Statistical Analysis of the Effects of Vertical Wind Shear on Tropical Cyclone Intensity Change over the Western North Pacific. *Mon. Weather Rev.*, **143**, 3434–3453, https://doi.org/10.1175/MWR-D-15-0049.1.

——, Y. Li, and J. Xu, 2021: A new time-dependent theory of tropical cyclone intensification. *J. Atmospheric Sci.*, **78**, 3855–3865, https://doi.org/10.1175/JAS-D-21-0169.1.

Weber, H. C., C. C. F. Lok, N. E. Davidson, and Y. Xiao, 2014: Objective Estimation of the Radius of the Outermost Closed Isobar in Tropical Cyclones. *Trop. Cyclone Res. Rev.*, **3**, 1–21, https://doi.org/10.6057/2014TCRR01.01.

Wing, A. A., S. J. Camargo, and A. H. Sobel, 2016: Role of Radiative–Convective Feedbacks in Spontaneous Tropical Cyclogenesis in Idealized Numerical Simulations. *J. Atmospheric Sci.*, **73**, 2633–2642, https://doi.org/10.1175/JAS-D-15-0380.1.

Wu, C.-C., T.-S. Huang, W.-P. Huang, and K.-H. Chou, 2003: *A New Look at the Binary Interaction: Potential Vorticity Diagnosis of the Unusual Southward Movement of Tropical Storm Bopha (2000) and Its Interaction with Supertyphoon Saomai (2000)*.

Wu, Q., and Z. Ruan, 2021: Rapid Contraction of the Radius of Maximum Tangential Wind and Rapid Intensification of a Tropical Cyclone. *J. Geophys. Res. Atmospheres*, **126**, https://doi.org/10.1029/2020JD033681.

Wu, S., and J. Fang, 2023: The Initial Mesoscale Vortexes Leading to the Formation of Tropical Cyclones in the Western North Pacific. *Adv. Atmospheric Sci.*, **40**, 804–823, https://doi.org/10.1007/s00376-022-2029-y.

Xu, J., and Y. Wang, 2010: Sensitivity of the simulated tropical cyclone inner-core size to the initial vortex size. *Mon. Weather Rev.*, **138**, 4135–4157, https://doi.org/10.1175/2010MWR3335.1.

——, and ——, 2015: A statistical analysis on the dependence of tropical cyclone intensification rate on the storm intensity and size in the North Atlantic. *Weather Forecast.*, **30**, 692–701, https://doi.org/10.1175/WAF-D-14-00141.1.

——, and ——, 2018a: Dependence of tropical cyclone intensification rate on sea surface temperature, storm intensity, and size in the Western North Pacific. *Weather Forecast.*, **33**, 523–537, https://doi.org/10.1175/WAF-D-17-0095.1.

——, and ——, 2018b: Effect of the initial vortex structure on intensification of a numerically simulated tropical cyclone. *J. Meteorol. Soc. Jpn.*, **96**, 111–126, https://doi.org/10.2151/jmsj.2018-014.

Xu, Y., T. Li, and M. Peng, 2013: Tropical Cyclogenesis in the Western North Pacific as Revealed by the 2008-09 YOTC Data. *Weather Forecast.*, **28**, 1038–1056, https://doi.org/10.1175/WAF-D-12-00104.1.

Yoshida, R., and H. Ishikawa, 2013: Environmental factors contributing to tropical cyclone genesis over the western north pacific. *Mon. Weather Rev.*, **141**, 451–467, https://doi.org/10.1175/MWR-D-11-00309.1.

——, Y. Kajikawa, and H. Ishikawa, 2014: Impact of Boreal Summer Intraseasonal Oscillation on Environment of Tropical Cyclone Genesis over the Western North Pacific. *Sola*, **10**, 15–18, https://doi.org/10.2151/sola.2014-004.

Zhao, K., H. Zhao, G. B. Raga, R. Yoshida, W. Wang, and P. J. Klotzbach, 2021: Changes in extended boreal summer tropical cyclogenesis associated with large-scale flow patterns over the western North Pacific in response to the global warming hiatus. *Clim. Dyn.*, **56**, 515–535, https://doi.org/10.1007/s00382-020-05486-x.

Tables

Table 3.1 Number of cases for each genesis type classified by objective method in this study and subjective method in Ritchie and Holland (1999).

		Objective					
		EW	MC	MS	MD	ALL	Percentage
	EW	60	15			75	80
	MC	1	101	6	2	110	91.8
	MS	5	27	81	13	126	64.3
Subjective	MD				65	65	100
	ALL	66	143	87	80	376	
	Percentage	90.9	70.6	93.1	81.2		

Figures
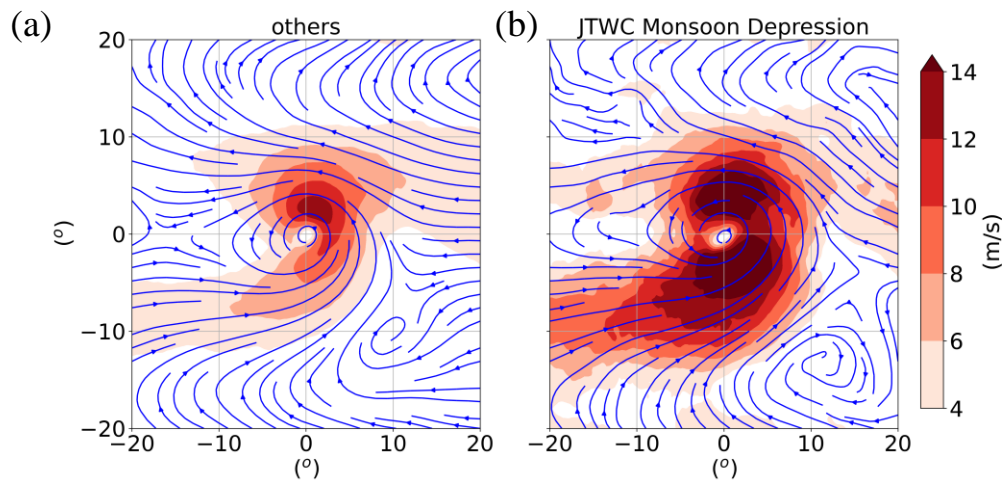
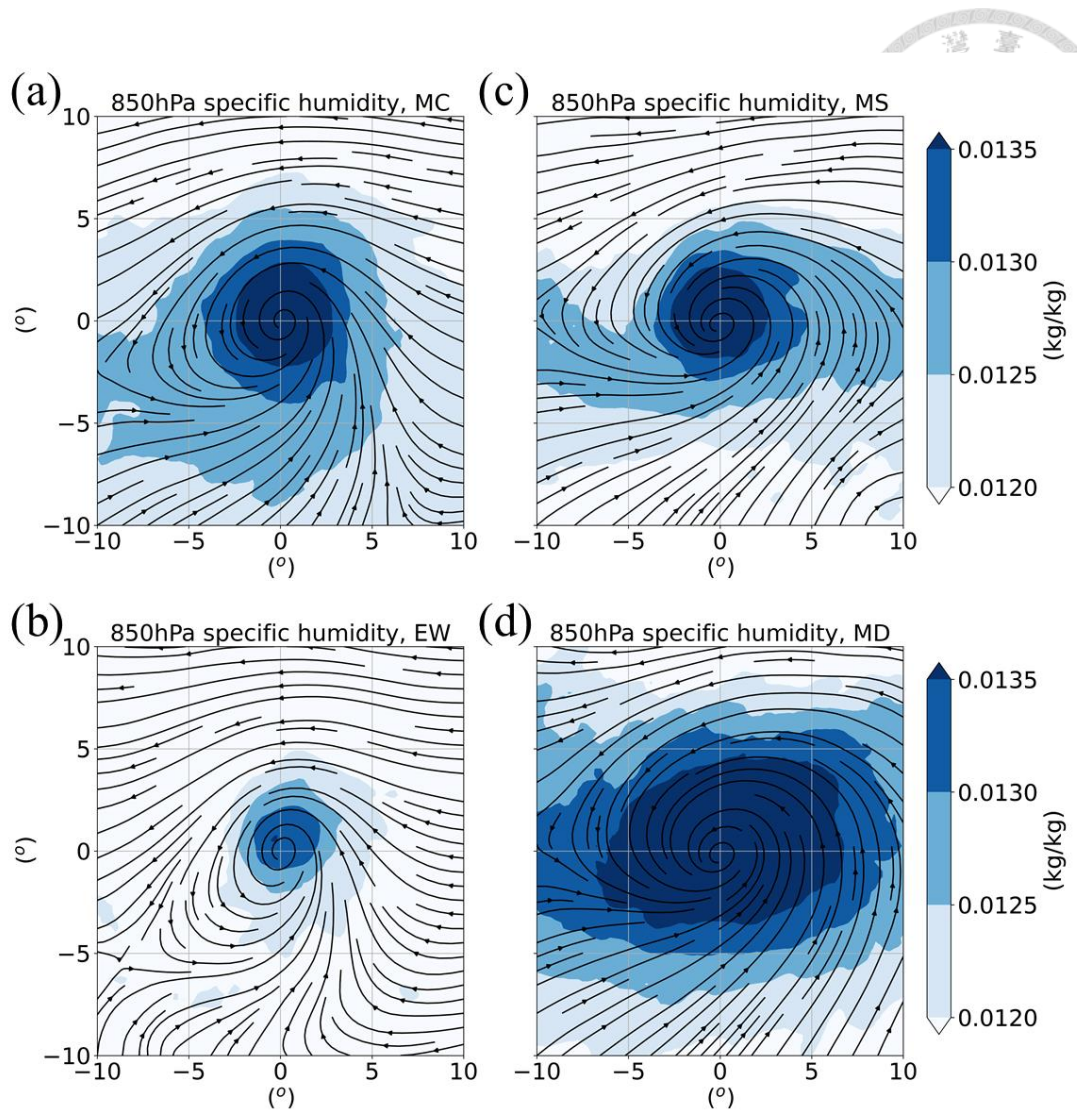Figure 1.1 850hPa wind field (streamline), and wind speed (shaded) composite of (b) 11 JTWC monsoon depression cases, (a) other cases
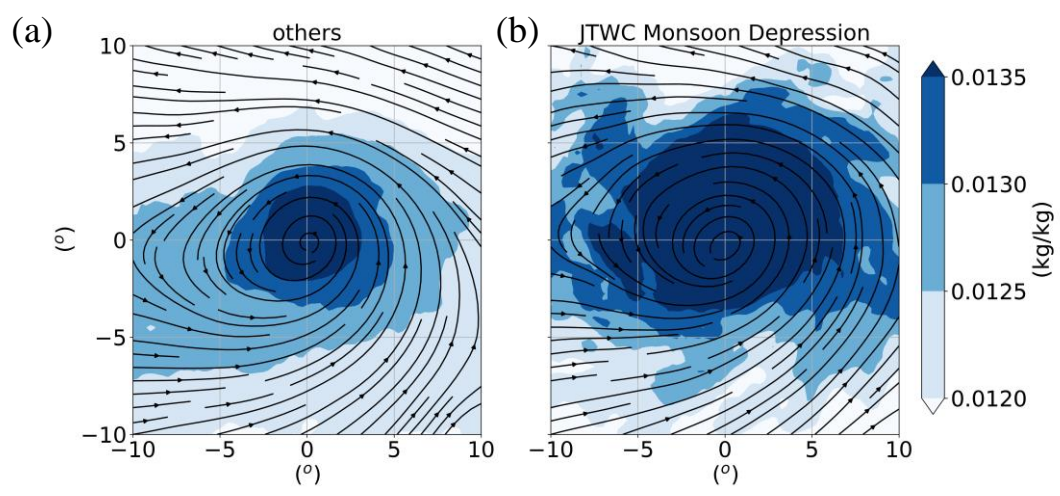
Figure 1.2 Similar to Fig. 1.1, but for 975hPa wind field (streamline) and 850hPa specific humidity (shaded).
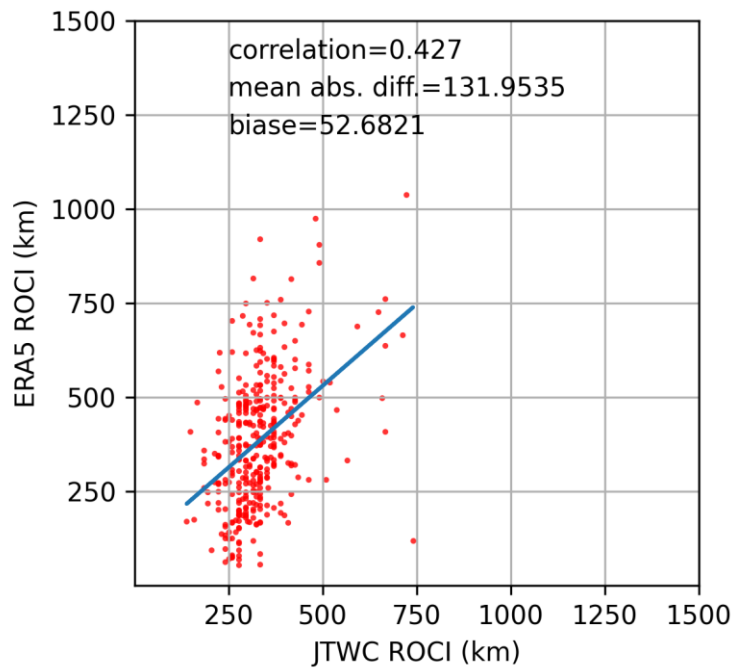
Figure 2.1 Scatter plot of the ROCI obtained from ERA5 and JTWC, blue line presents the regression line.
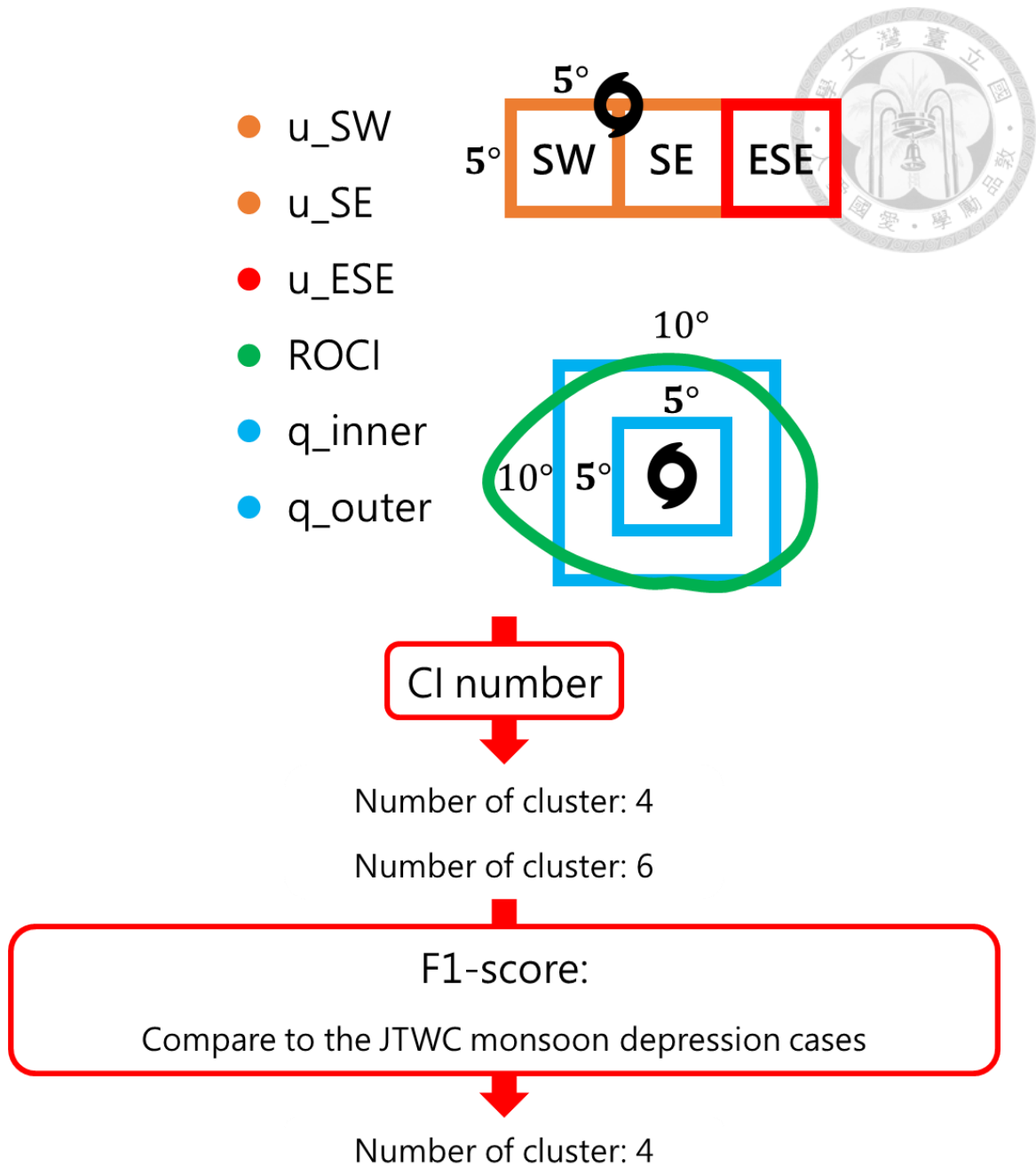
Figure 2.2 Flow chart of the objective method using K-maens cluster in this study.
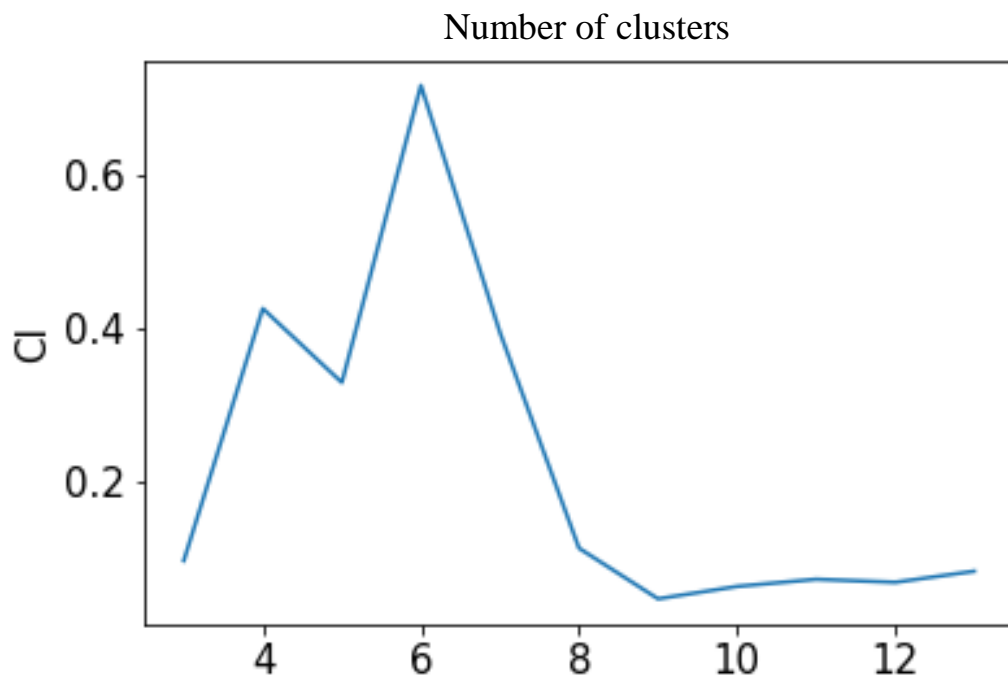
Figure 2.3 Line plot of the CI numbers in response to the number of clusters.

(a) GPH perturbation of TC (850 hPa), (EW)

(b) GPH perturbation of TC (850 hPa), (MD)
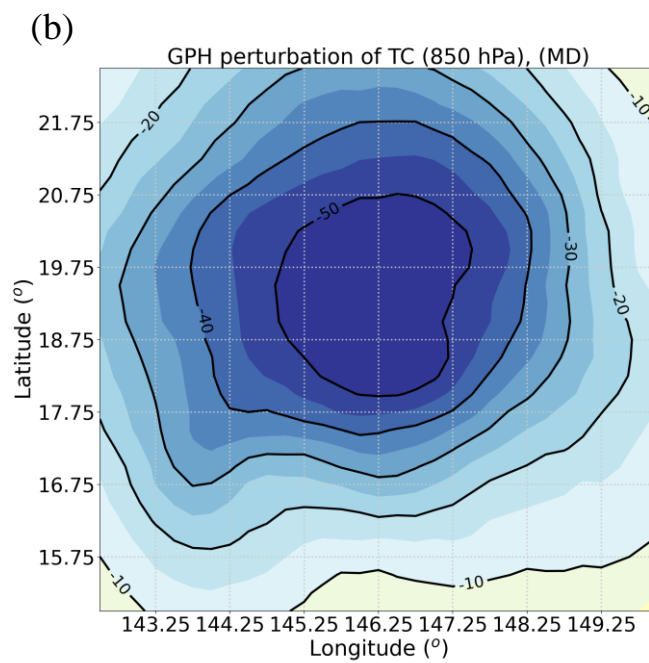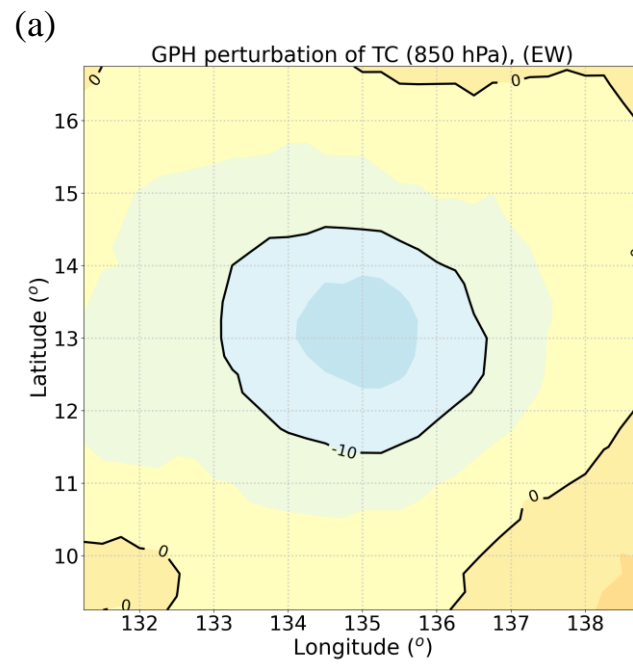
Figure 2.4 850hPa geopotential height perturbation of TCs in (a) EW and (b) MD experiments.
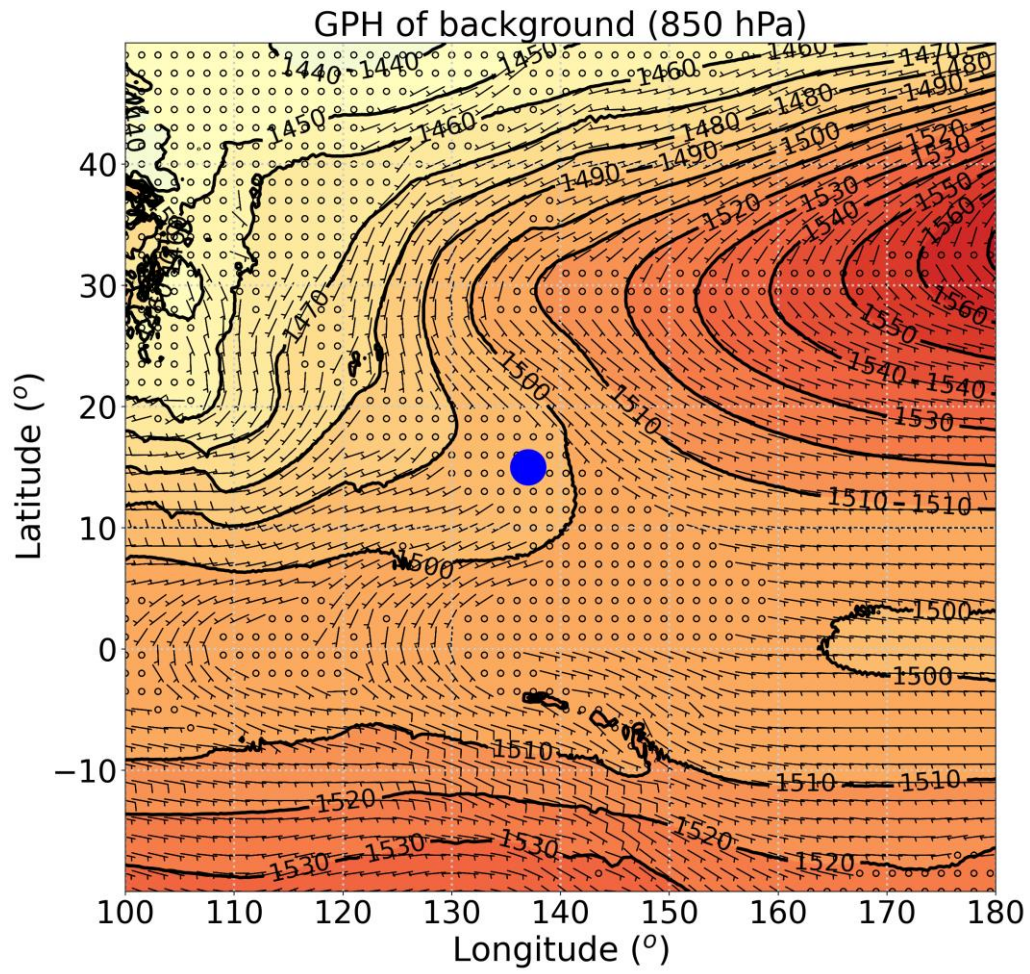
Figure 2.5 850hPa geopotential height field. Blue dot presents the location where TC is placed for numerical experiments.

(a)

I_RMW vs. Lifetime Max. Intensification Rate

$y=818.1278/x+21.1368$

○ 1 case
● 3 cases
● 5 cases

(b)

TS_RMW vs. Lifetime Max. Intensification Rate
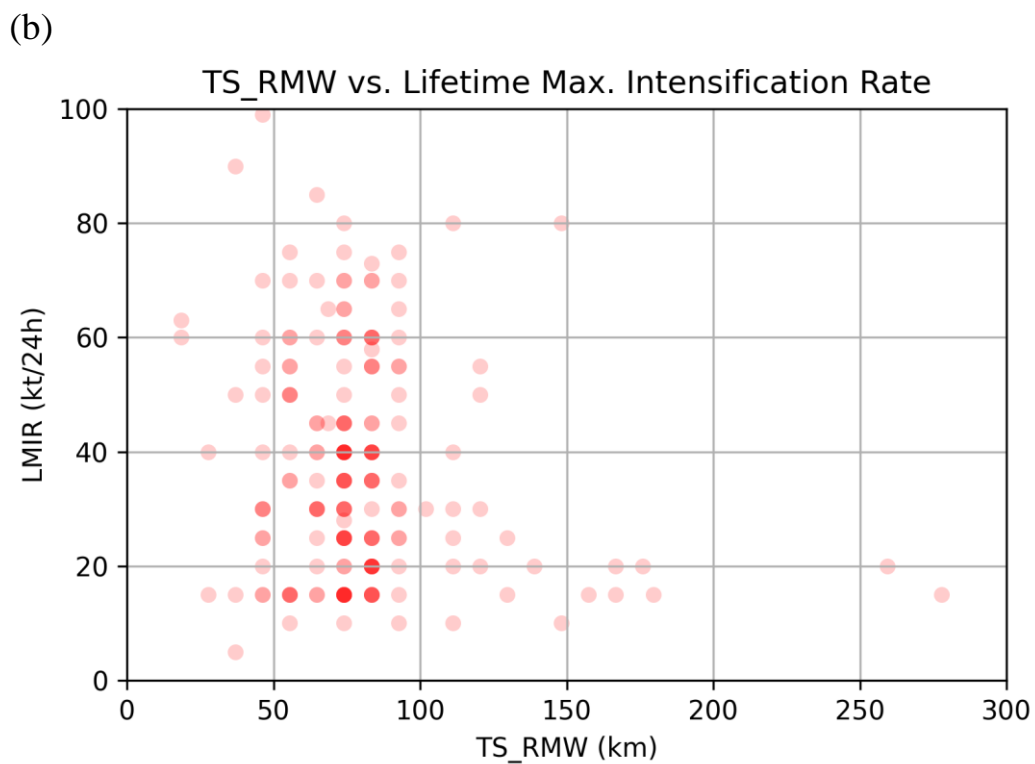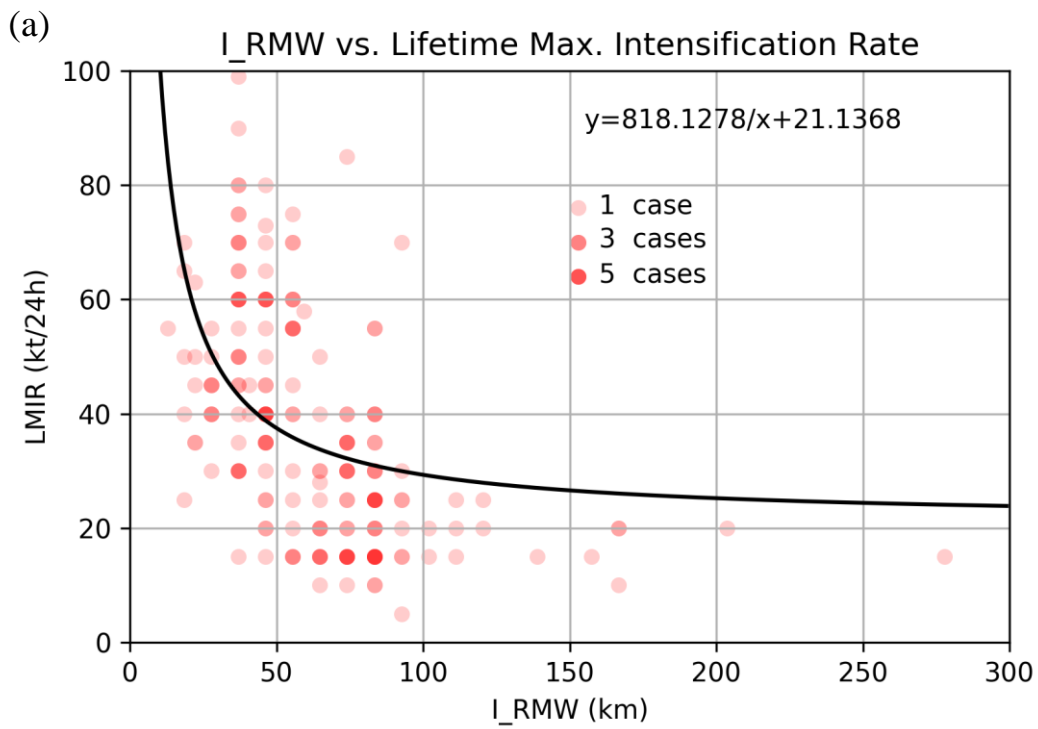
Figure 3.1 Scatter plots of LMIR and (a) I_RMW, and (b) TS_RMW. Black curve shows the regression line referenced from tangential wind tendency equation.
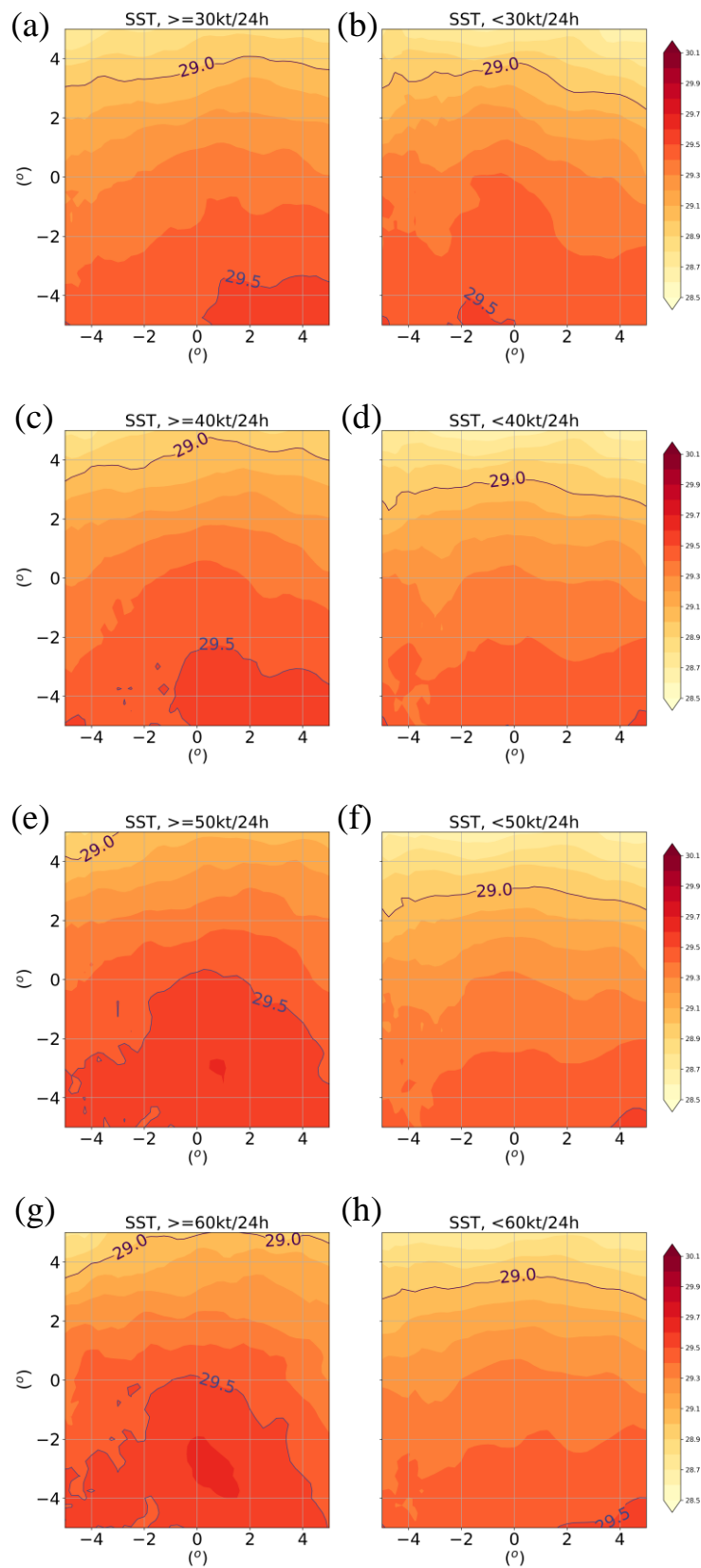
Figure 3.2 SST composites of different LMIR cases: (a) ≥30 knots per day, (b) <30 knots per day. (c) to (h) are similar to (a) and (b), but for 40-60 knots per day.
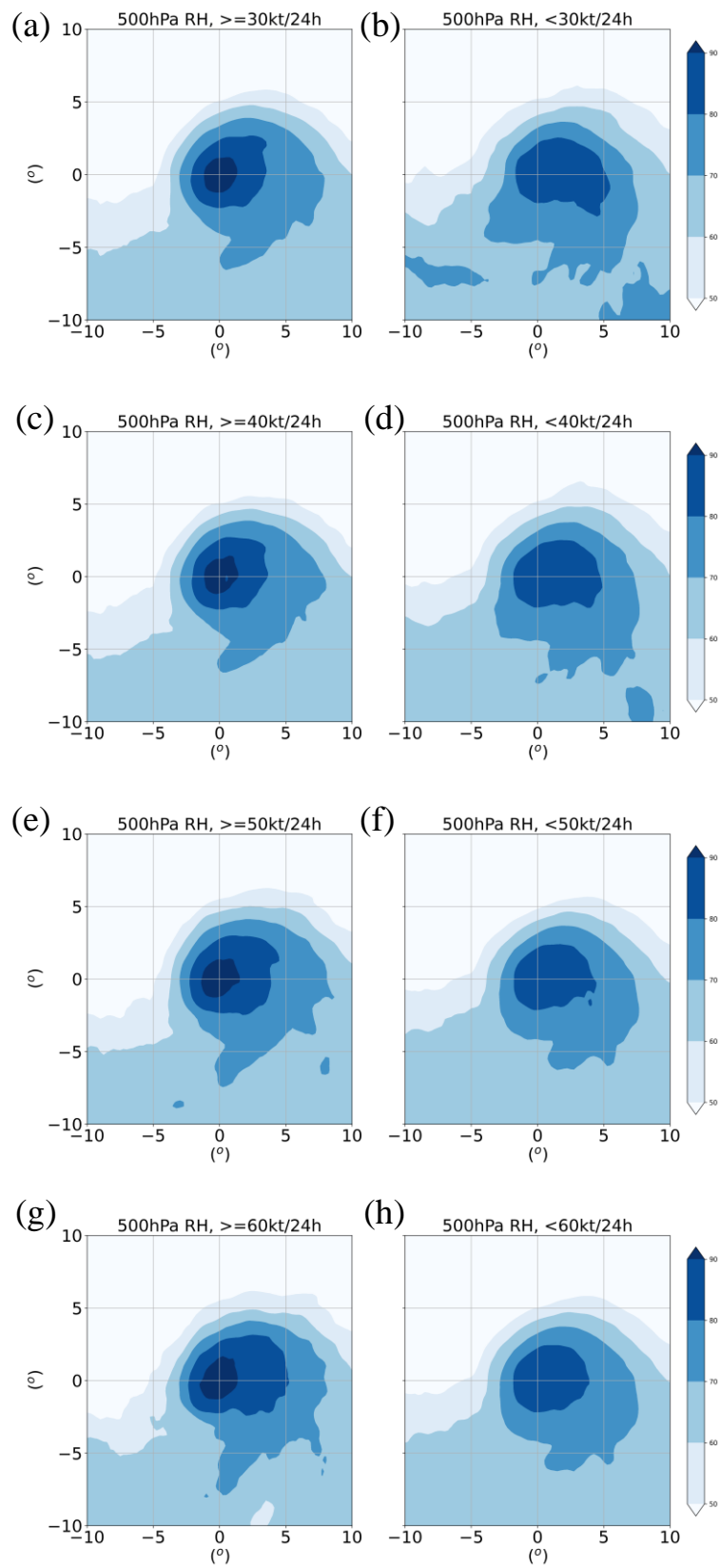
Figure 3.3 Similar to Fig. 3.3, but for 500hPa RH.

(a)

(b)

(c)
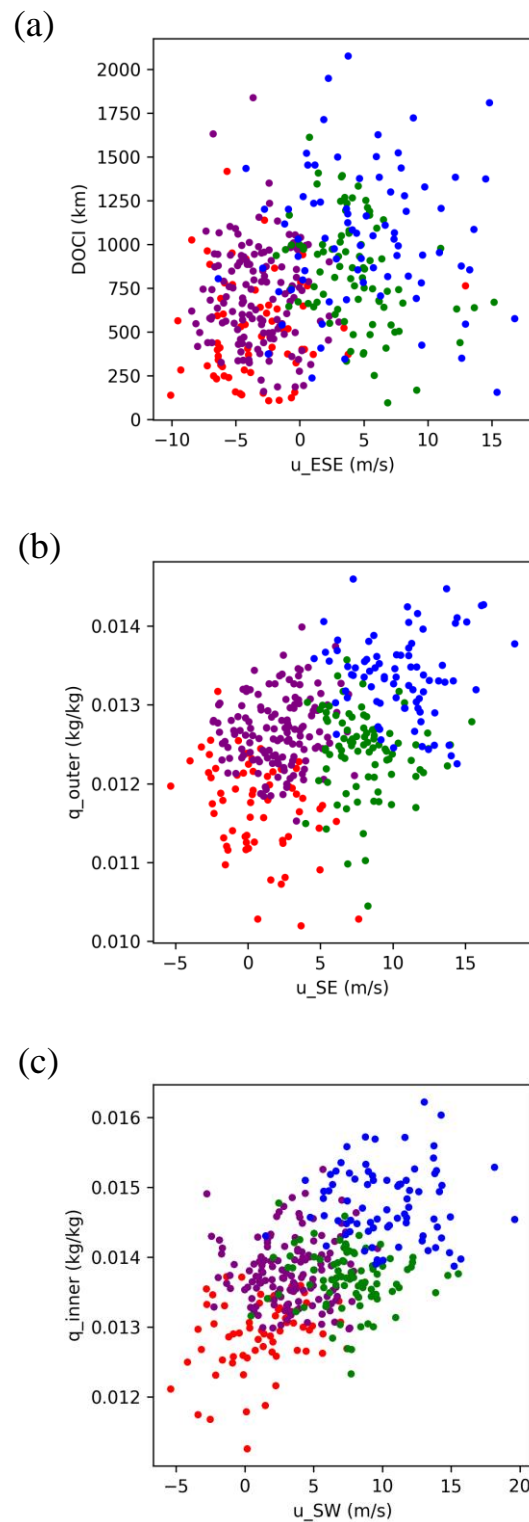
Figure 3.4 Scatter plots for (a) DOCI and u_ESE, (b) q_outer and u_ESE, and (c) q_inner and u_SW of each cases. Purple, red, green, and blue dots present the cases of type 1 to 4 respectively.
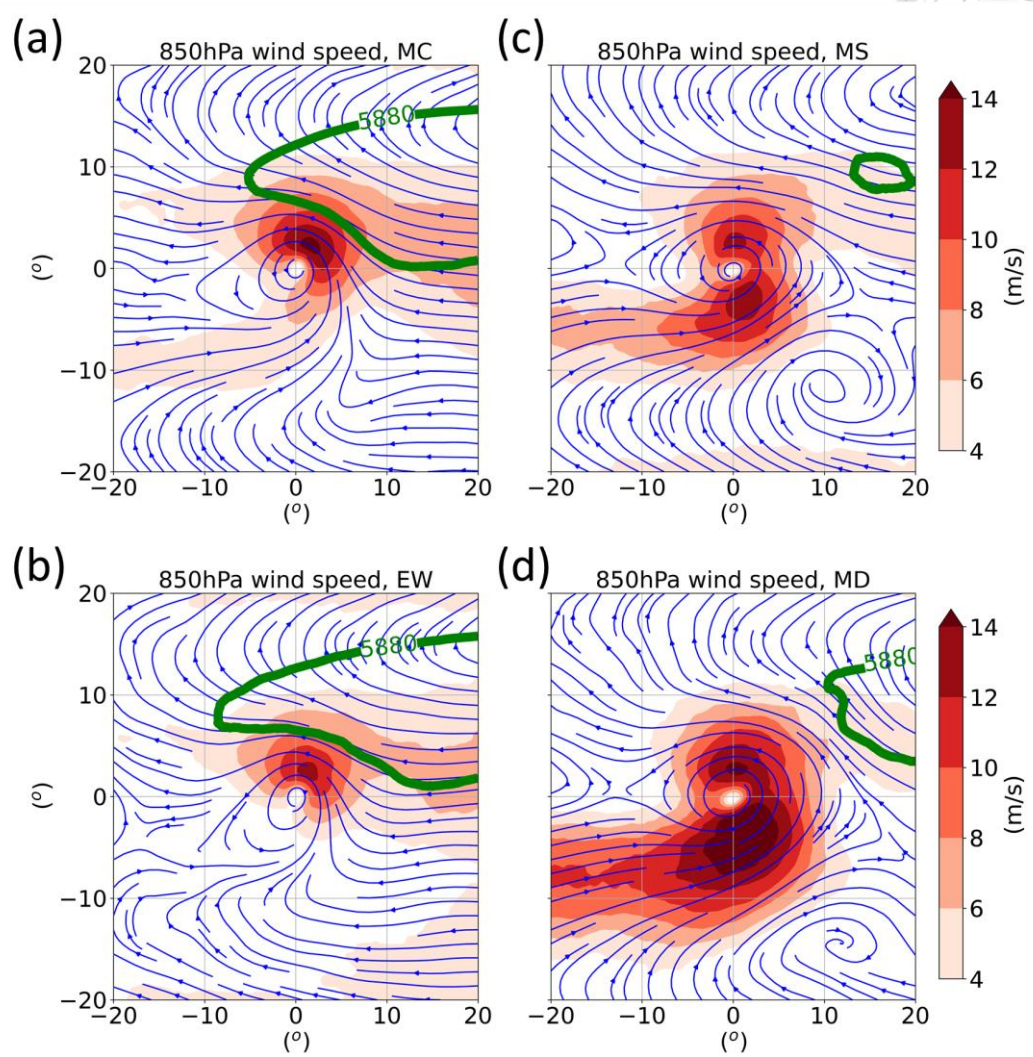
Figure 3.5 850hPa wind field (streamline), wind speed (shaded), and 500hPa geopotential height (contour) composite of (a) MC, (b) EW, (c) MS, and (d) MD.
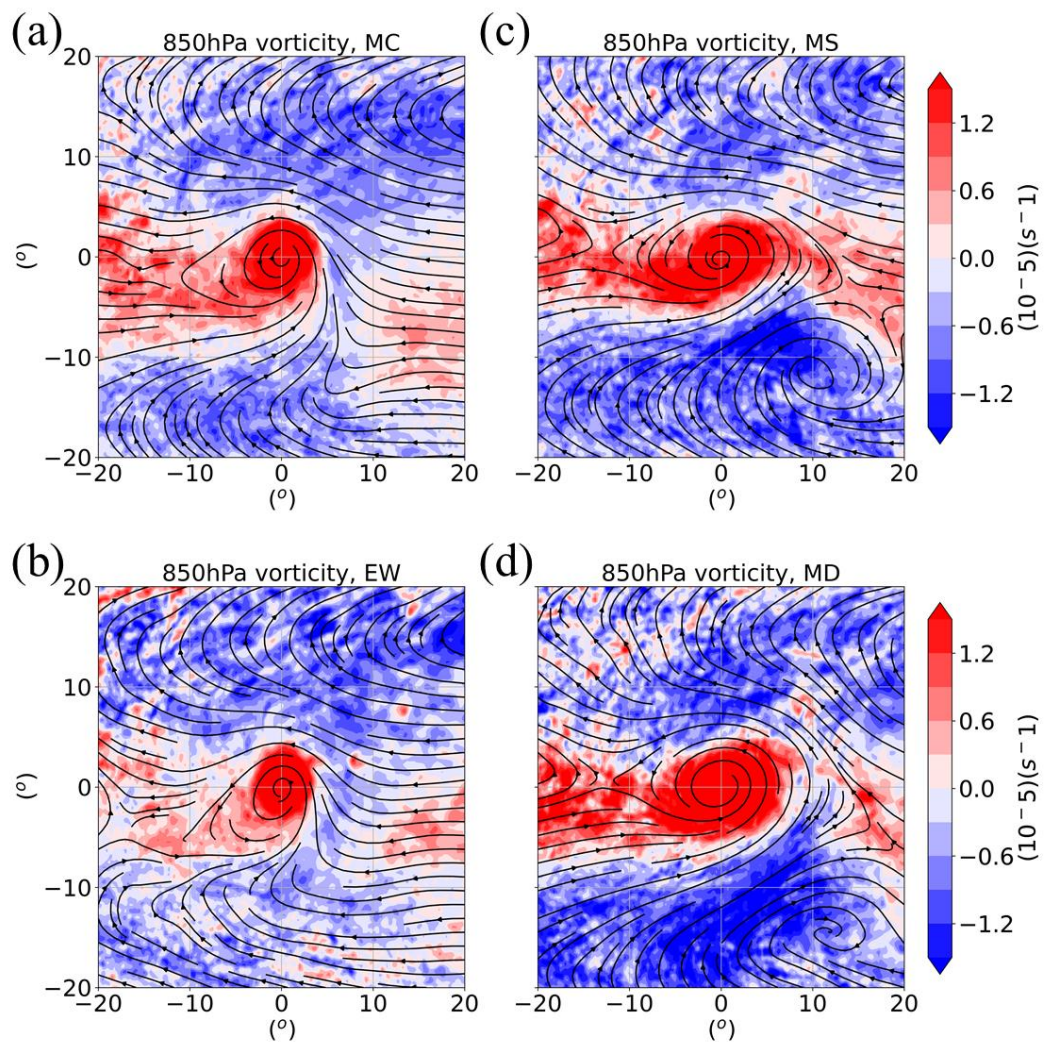
Figure 3.6 Similar to Fig. 3.5, but for 850hPa wind field (streamline) and vorticity (shaded).
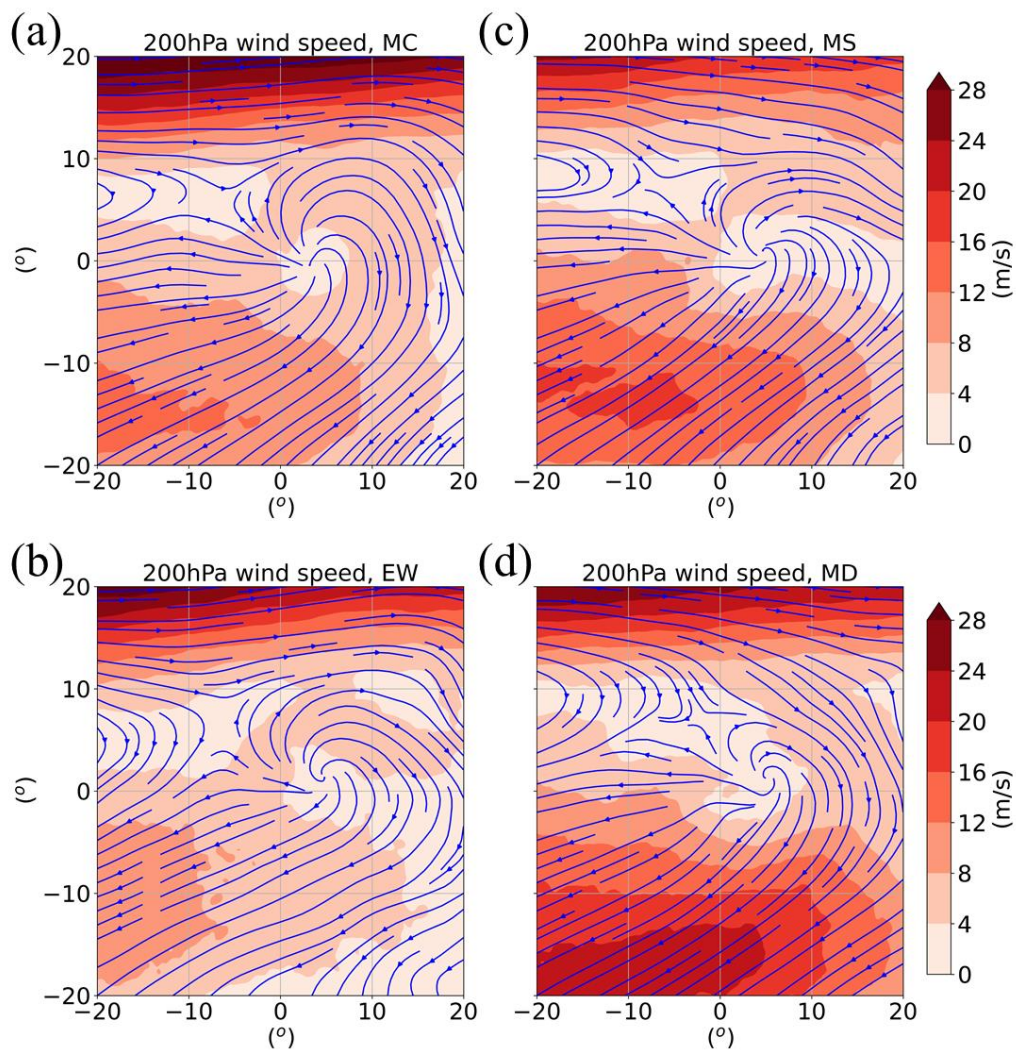
Figure 3.7 Similar to Fig. 3.5, but for 200hPa wind field (streamline) and wind speed (shaded).
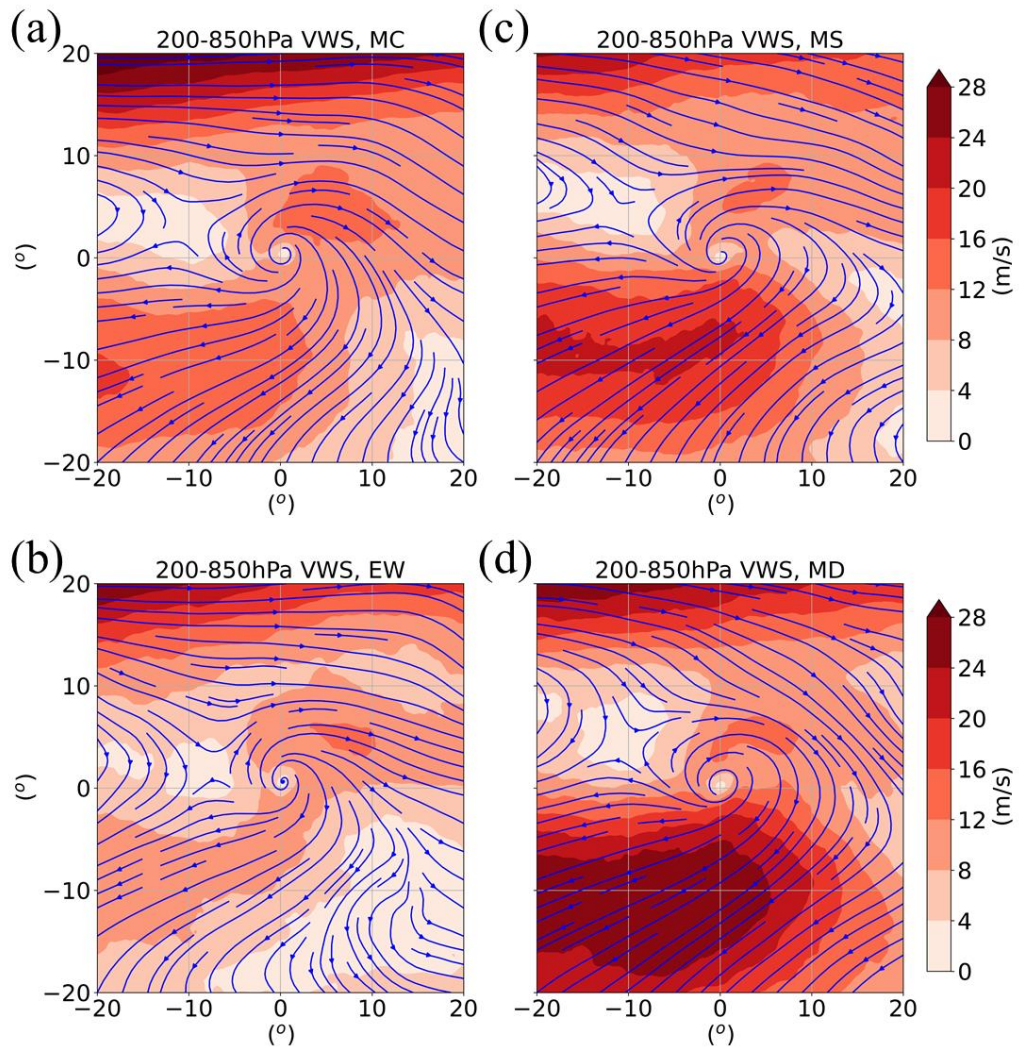
Figure 3.8 Similar to Fig. 3.5, but for 200-850hPa VWS field (streamline and shaded).
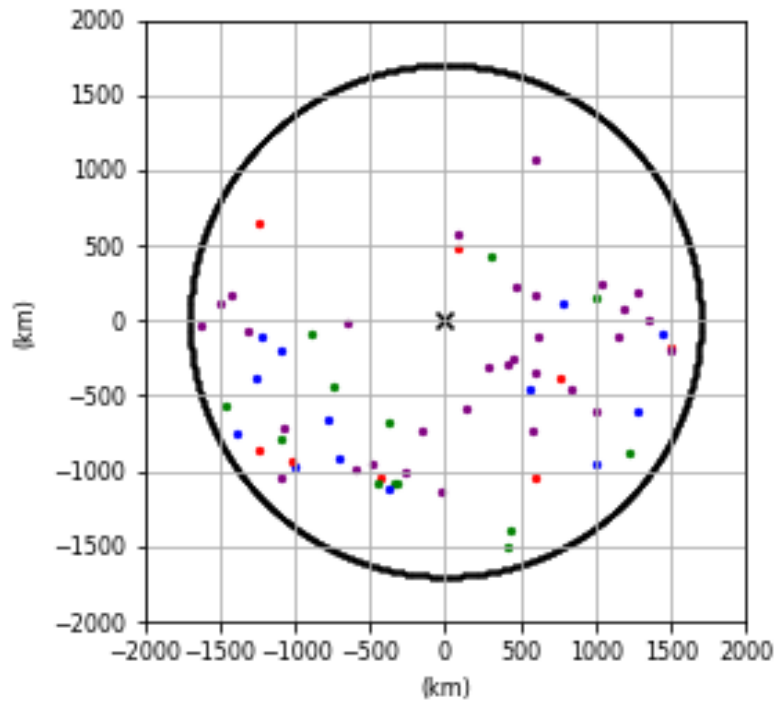
Figure 3.9 Similar to Fig. 3.4, but for the locations at TD_TIME related to locations of TUTT-cell. Black circle shows the radius of 1700km.

Figure 3.10 Similar to Fig. 3.5, but for 975hPa wind field (streamline) and 850hPa specific humidity (shaded).
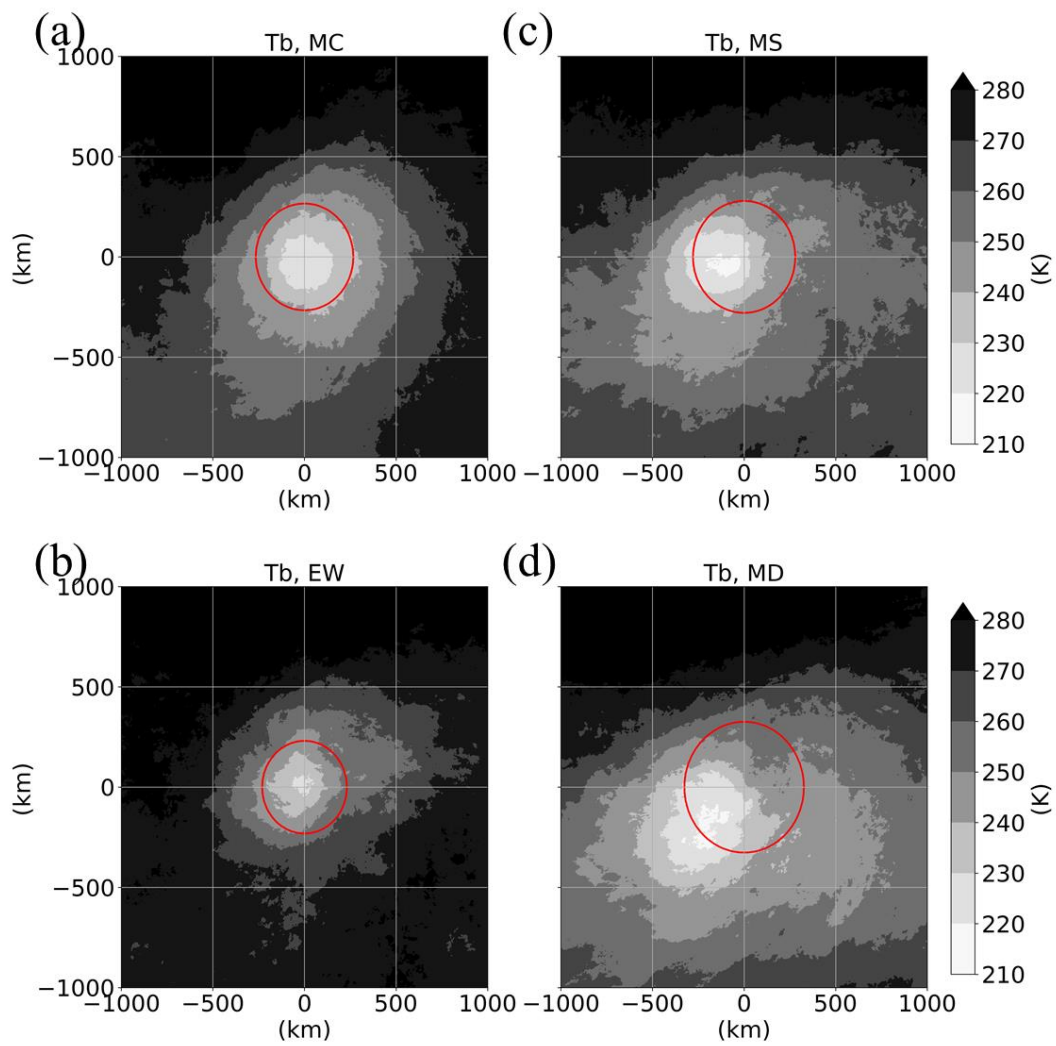
Figure 3.11 Similar to Fig. 3.5, but for brightness temperature (shaded) and mean RMW (red circle).

(a)

(b)

(c)

(d)
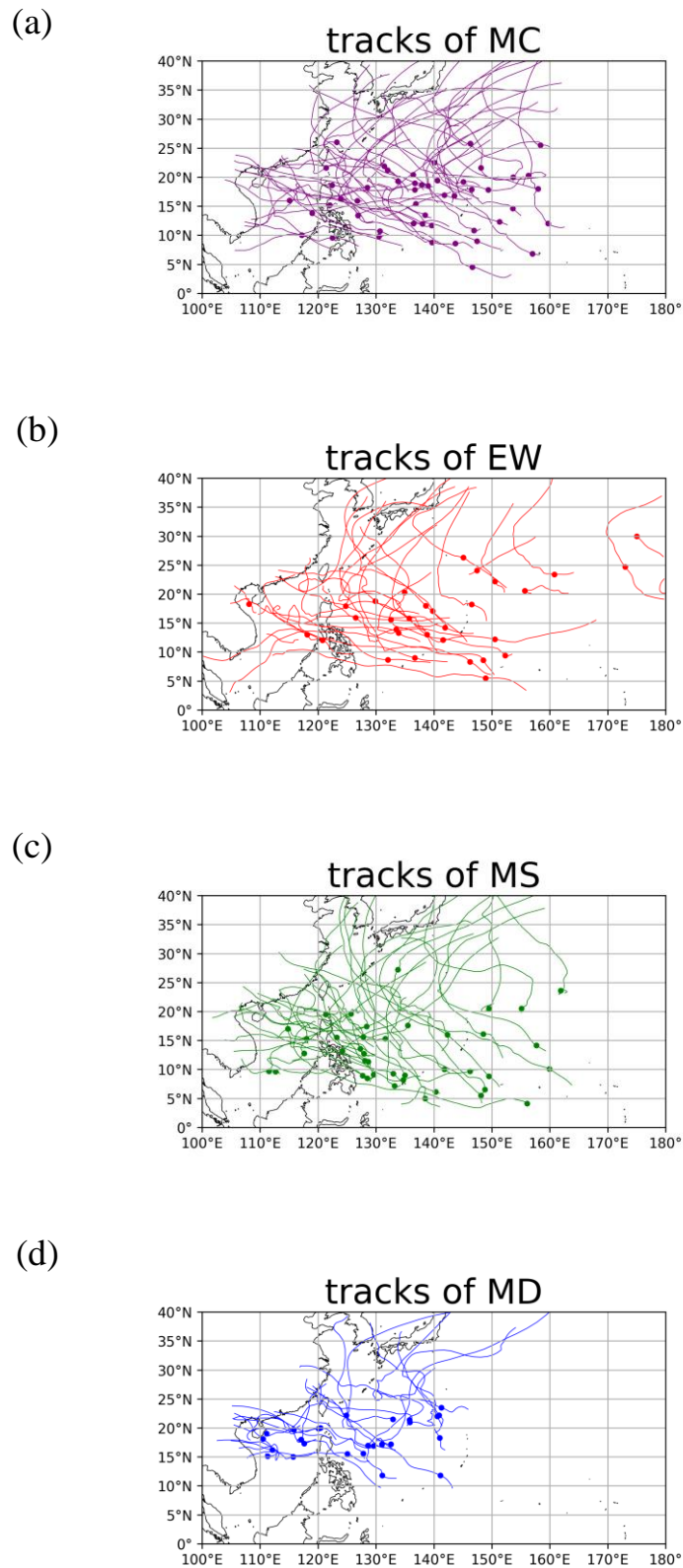
Figure 3.12 Tracks of cases from 2006-2012 in (a) MC, (b) EW, (c) MS, and (d) MD types. Dots present the locations at TD_TIME

(a)

(b)

(c)
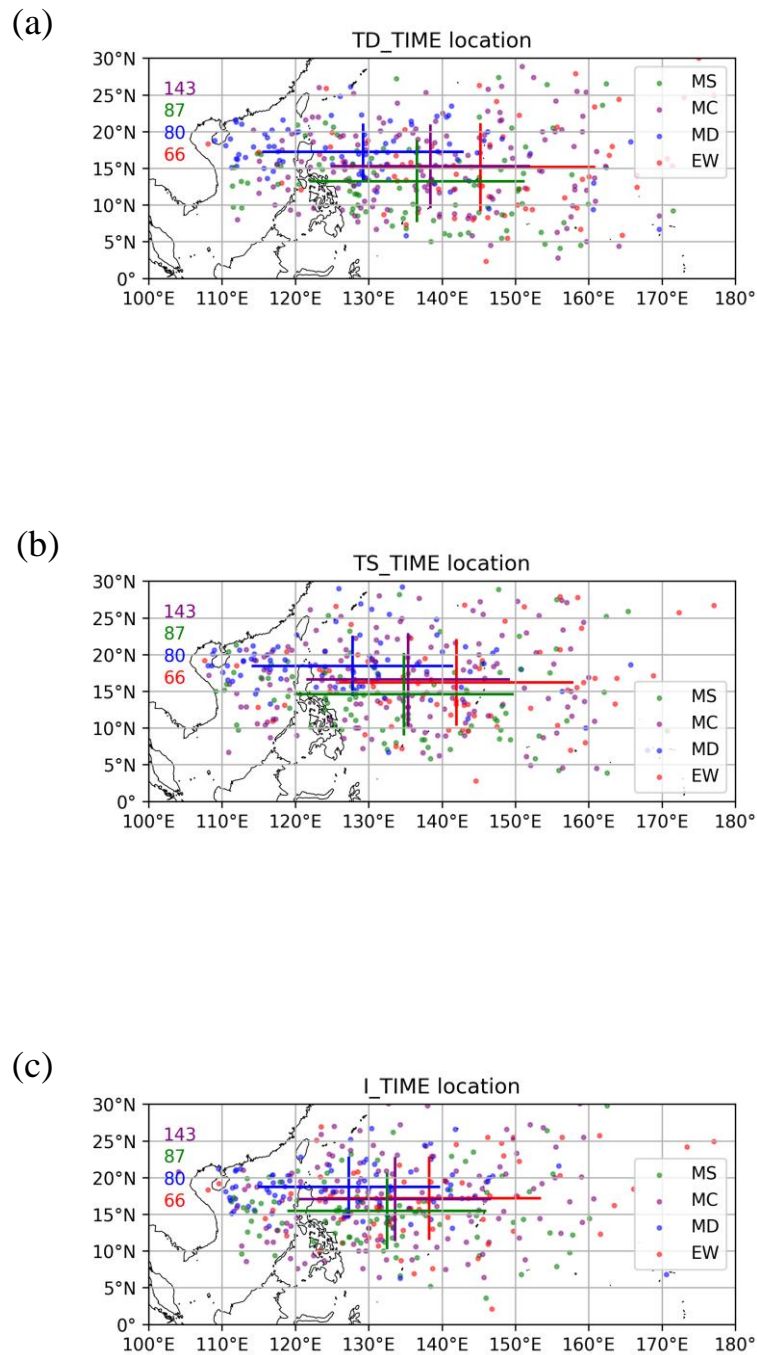
Figure 3.13 Locations of all cases at (a) TD_TIME, (b) TS_TIME, and (c) I_TIME. Number of cases is shown at the upper-left corner. Crosslines show the mean and 1 standard deviation of latitude and longtitude of locations in each genesis type.
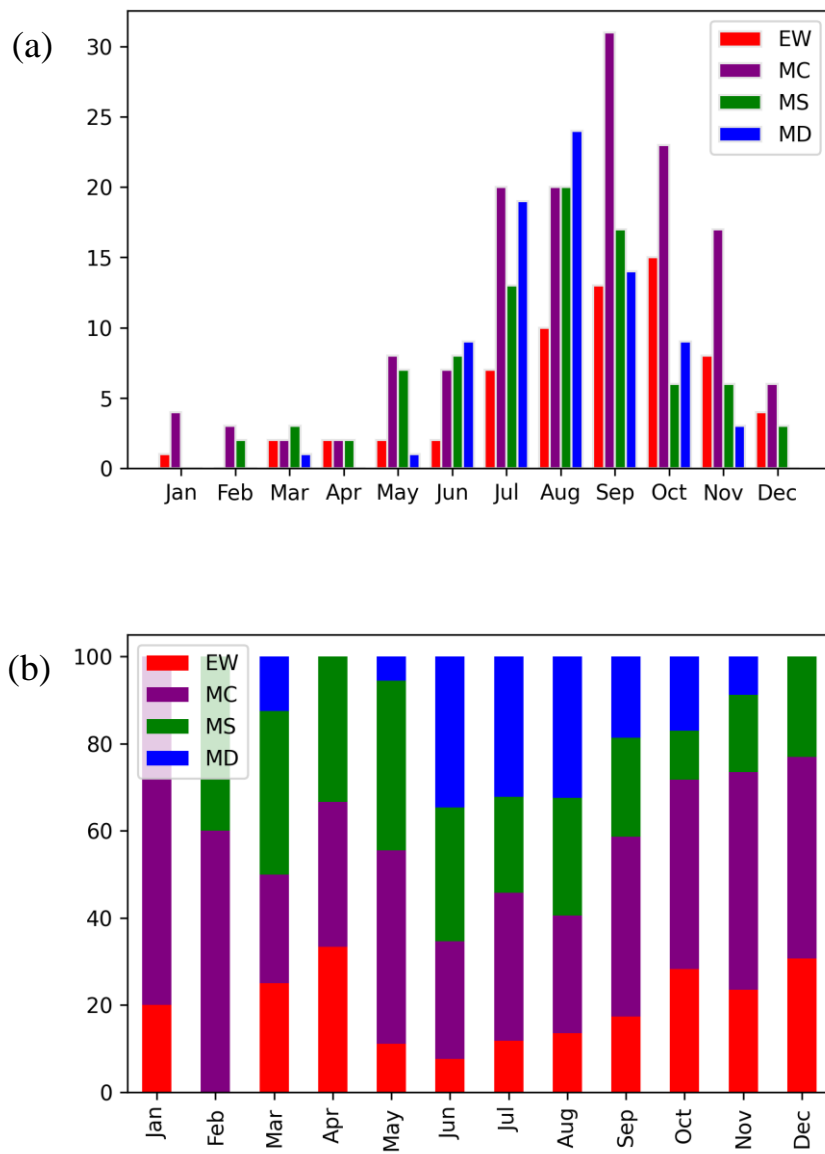
Figure 3.14 Seasonality of each genesis type in (a) number of cases, and (b) percentage.
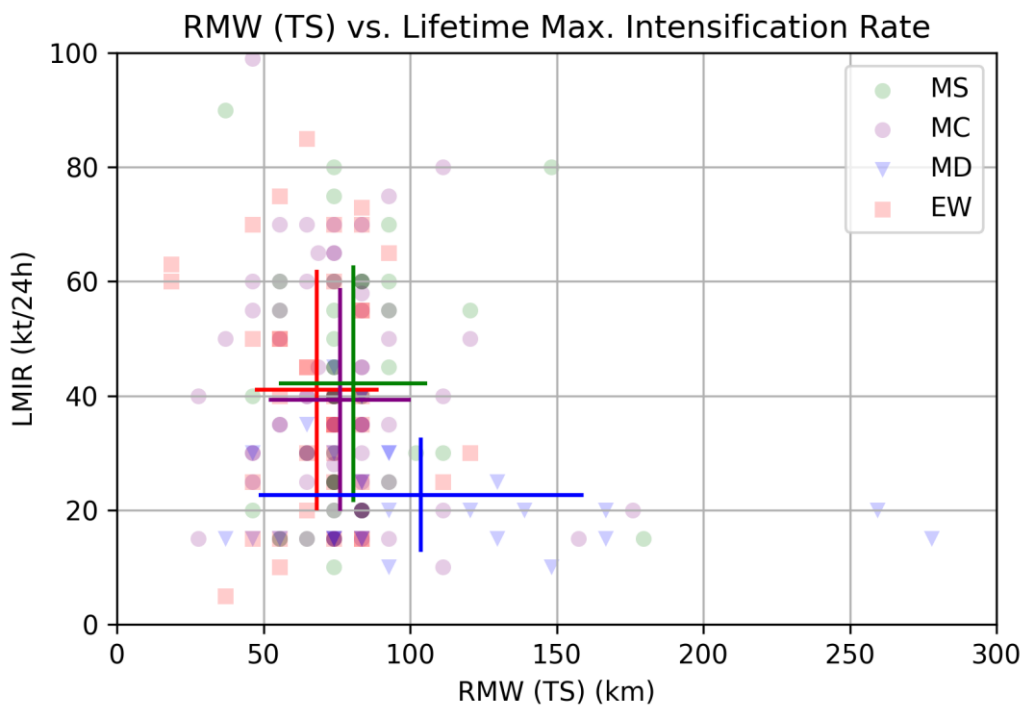
Figure 3.15 Similar to Fig. 3.13, but for scatter plots of LMIR and TS_RMW as shown in Fig. 3.1.
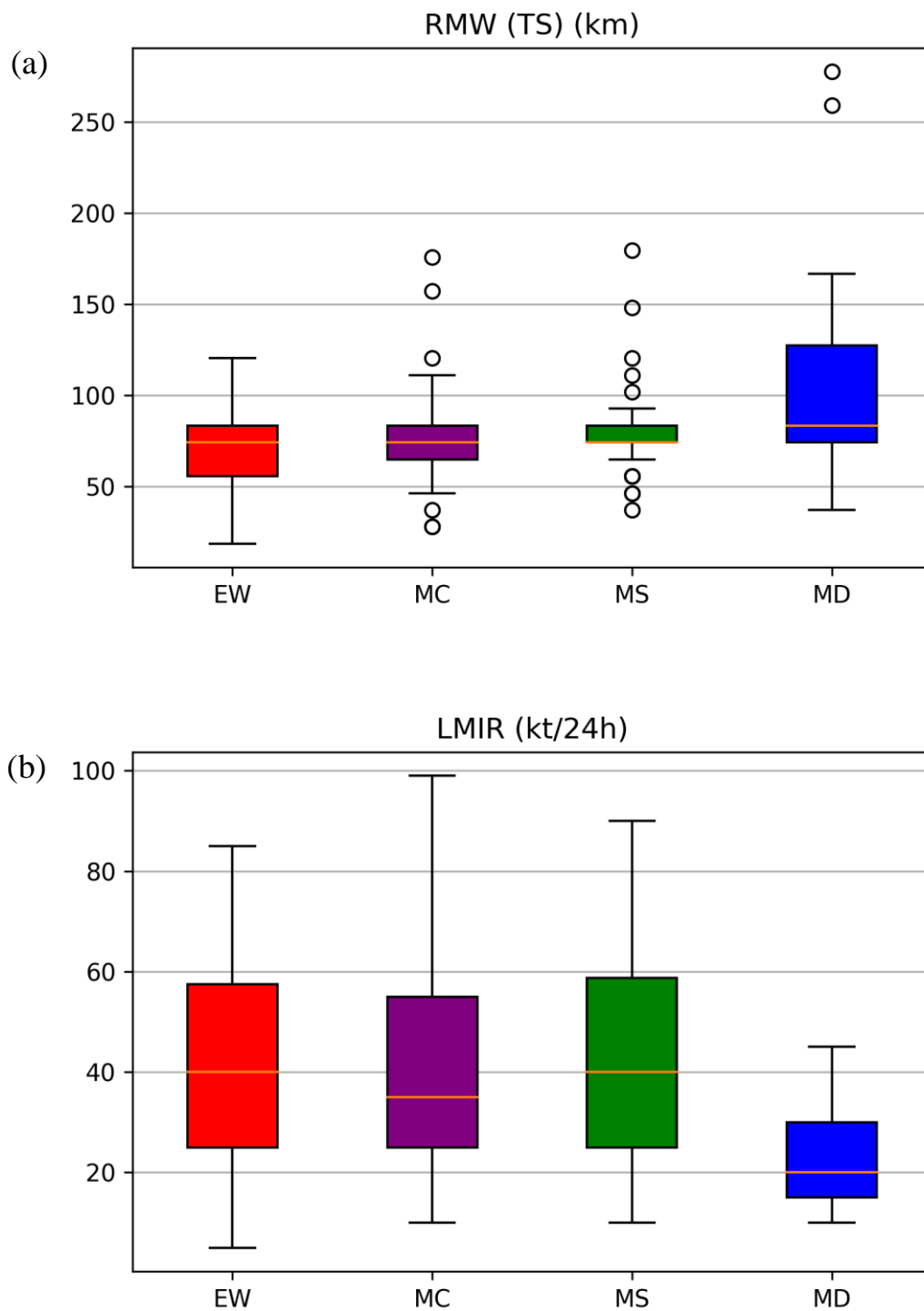
Figure 3.16 Boxplot of (a) TS_RMW, and (b) LMIR in four genesis types.

(a) 850hPa wind VAR, MC

(c) 850hPa wind VAR, MS

(b) 850hPa wind VAR, EW

(d) 850hPa wind VAR, MD
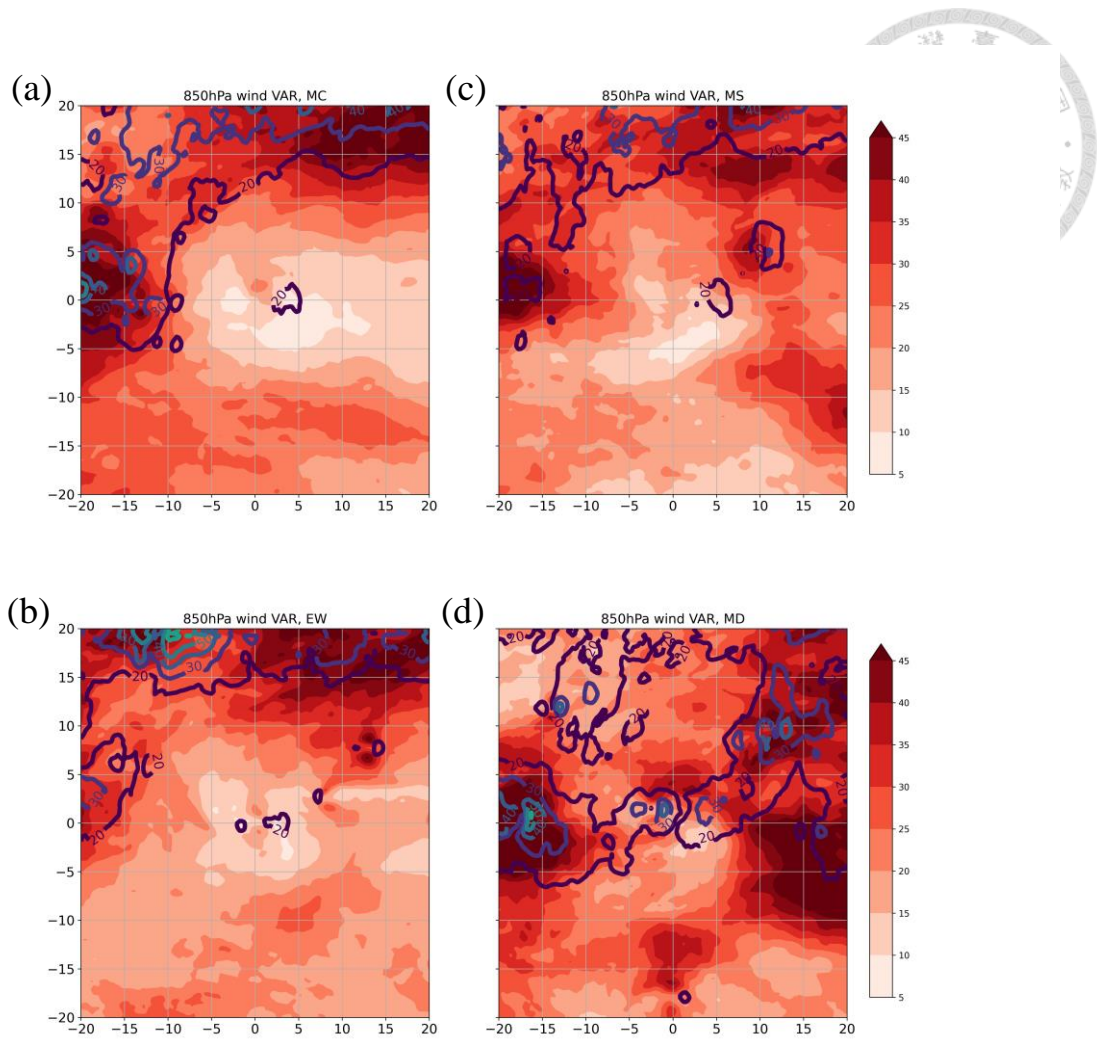
Figure 3.17 Similar to Fig. 3.5, but for variance of 850hPa zonal wind (shaded) and meridional wind (contour).
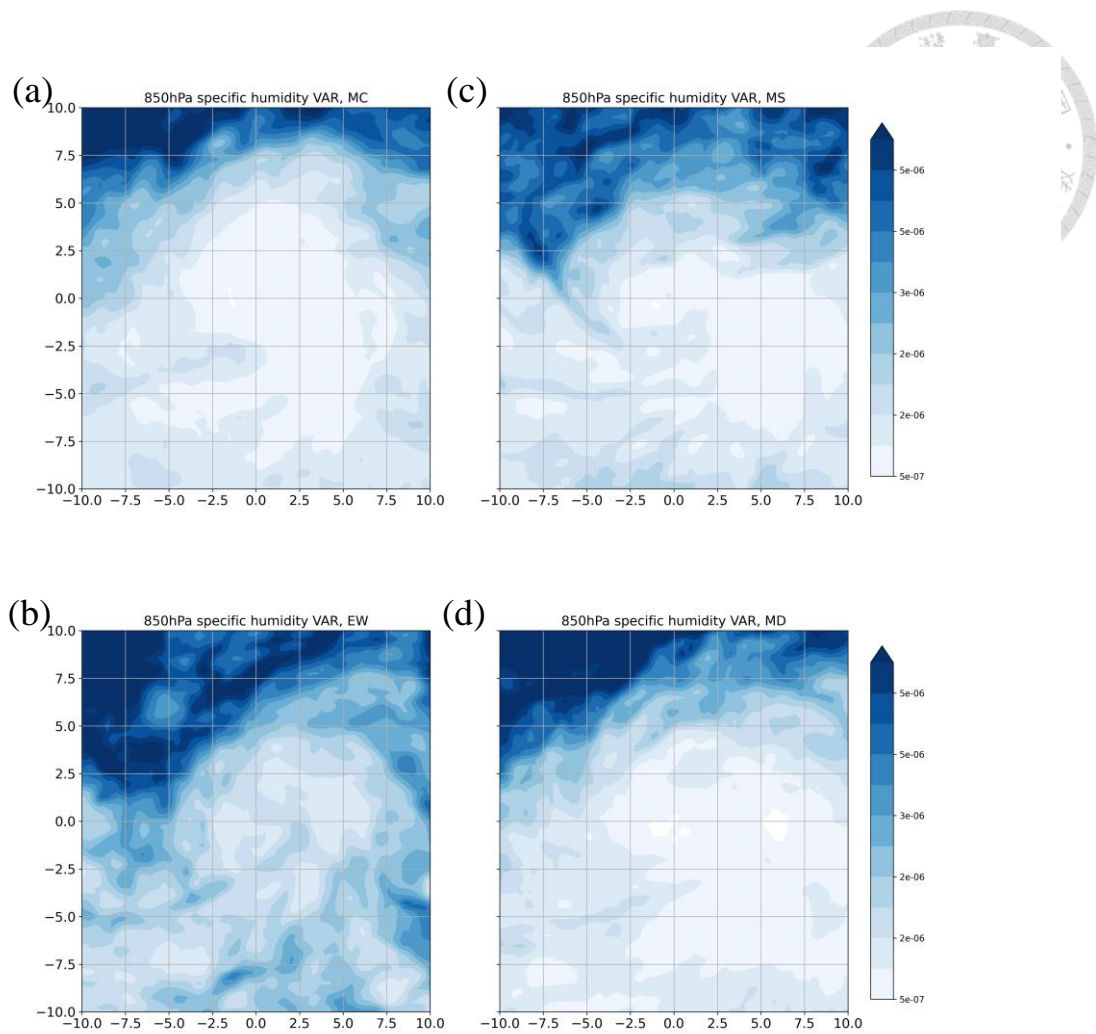
Figure 3.18 Similar to Fig. 3.5, but for variance of 850hPa specific humidity (shaded).
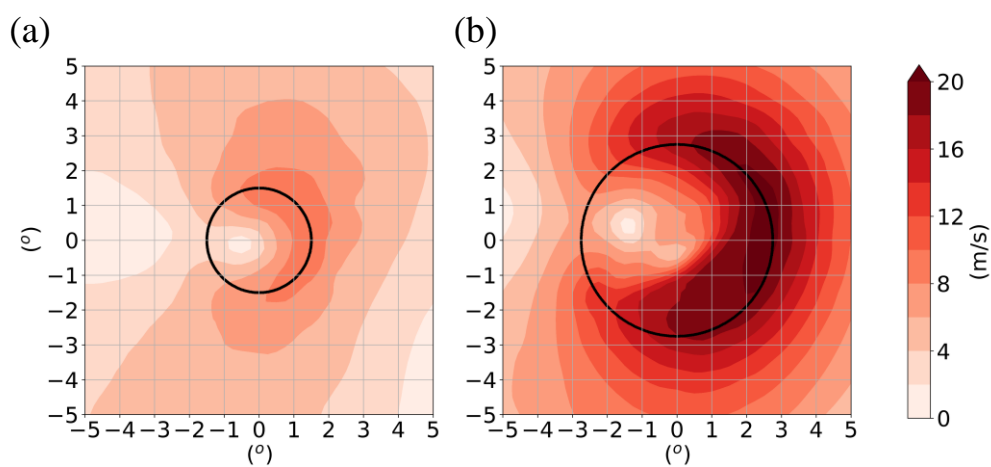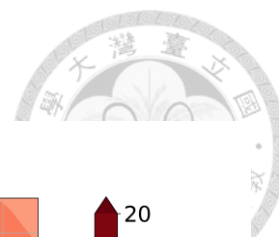
Figure 4.1 850hPa wind speed (shaded) of (a) EW and (b) MD in the initial field. Black circle shows the RMW.
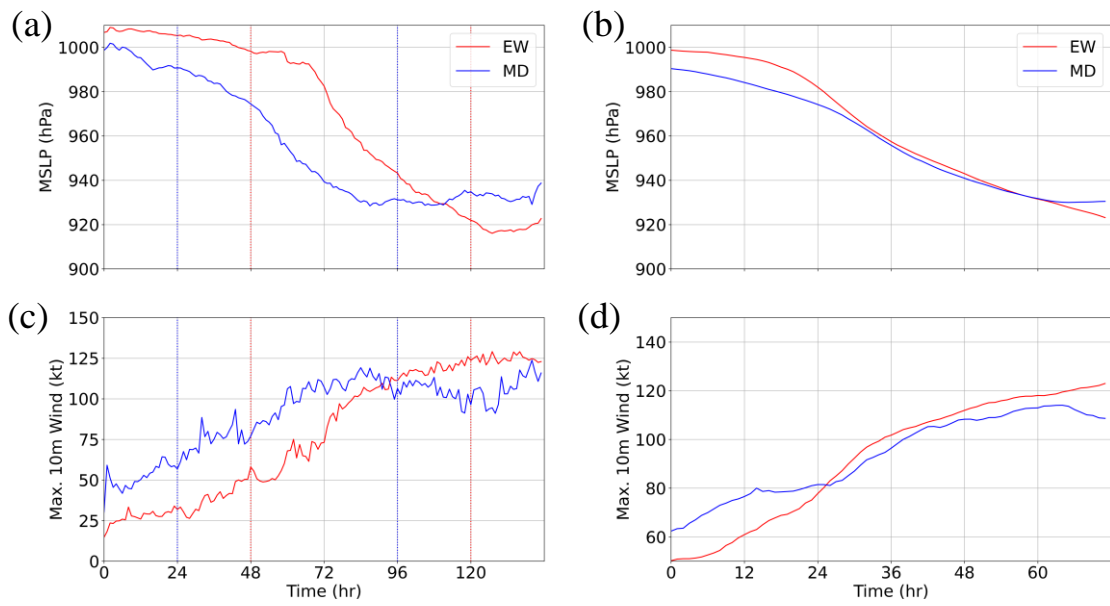
Figure 4.2 Time series of (a) sea level pressure, and (c) maximum wind speed of EW and MD experiments. (b) and (d) are similar to (a) and (c), but with the series between the dashed lines and calculated from the moving average over ±6 hours.
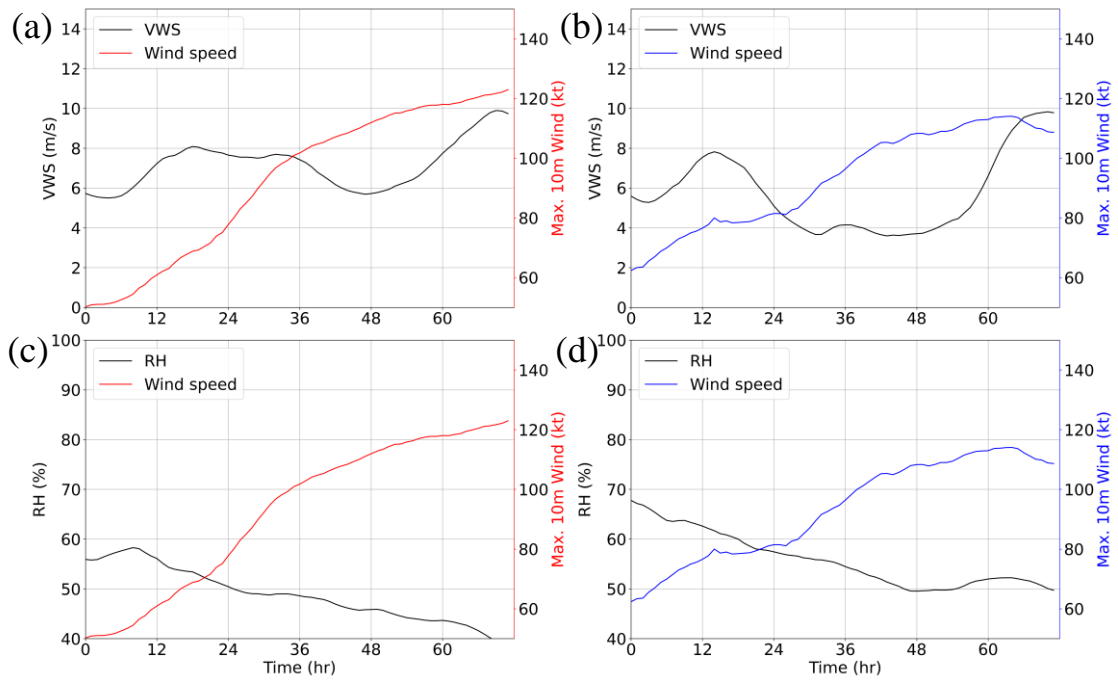
Figure 4.3 Time series of (a) and (b): VWS, (c) and (d): RH of EW and MD
experiments.
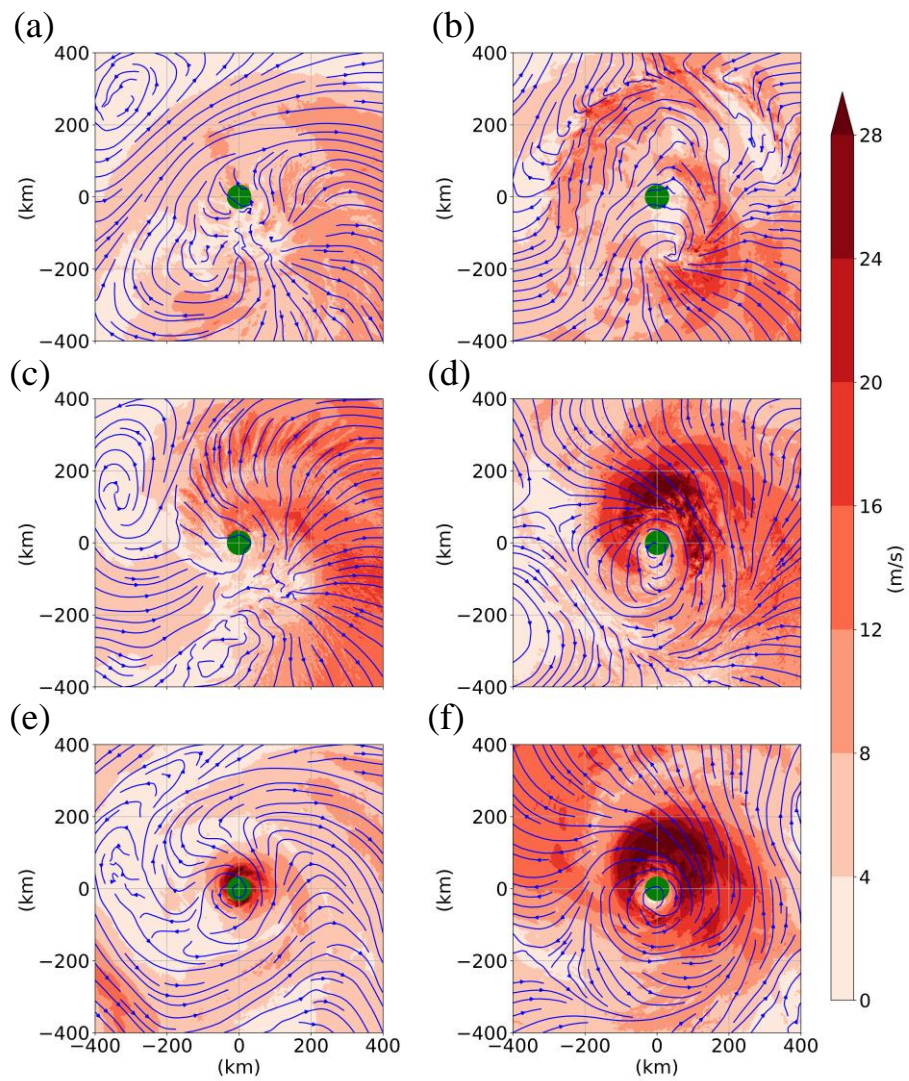
Figure 4.4 200hPa wind field (streamline) and wind speed (shaded) at the (a) 6 h, (c) 18 h, and (e) 30 h of EW experiment. (b), (d), (f) are similar to (a), (c), (e), but for MD experiment.
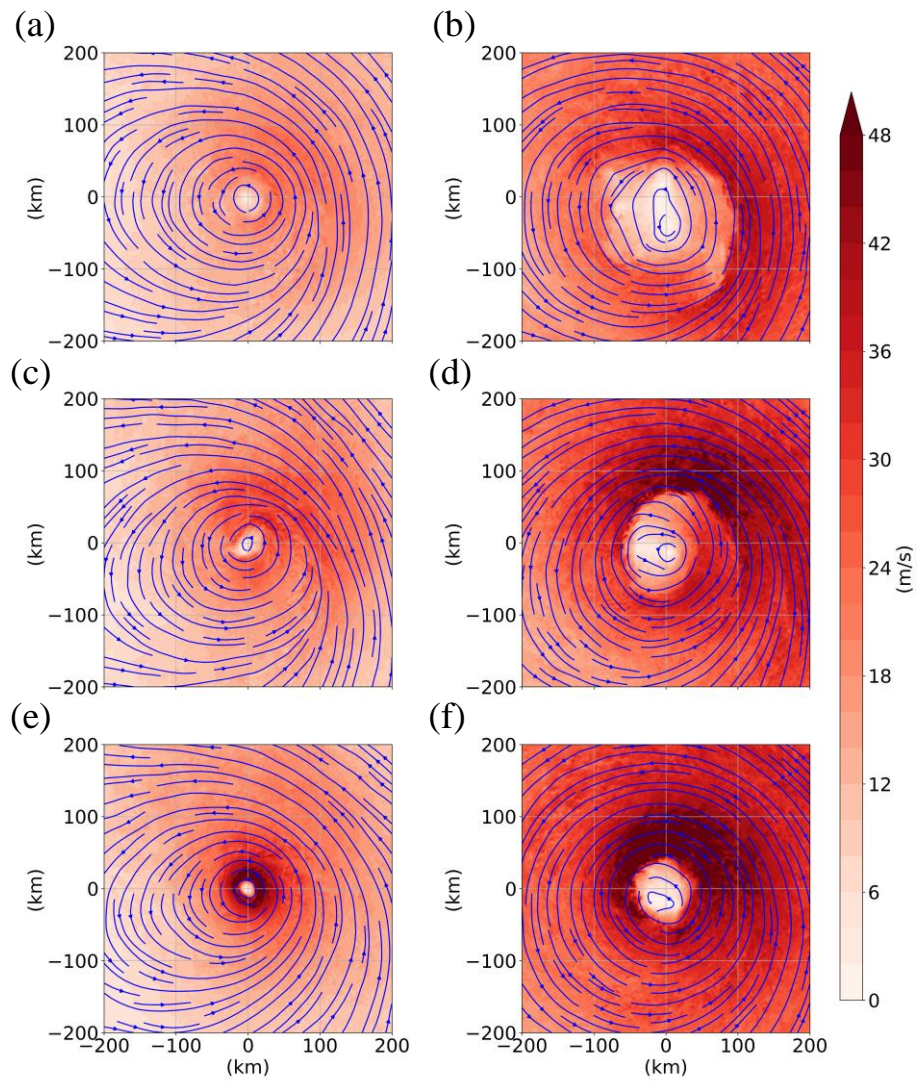
Figure 4.5 Similar to Fig. 4.4, but for 850hPa wind field (streamline) and wind speed (shaded).
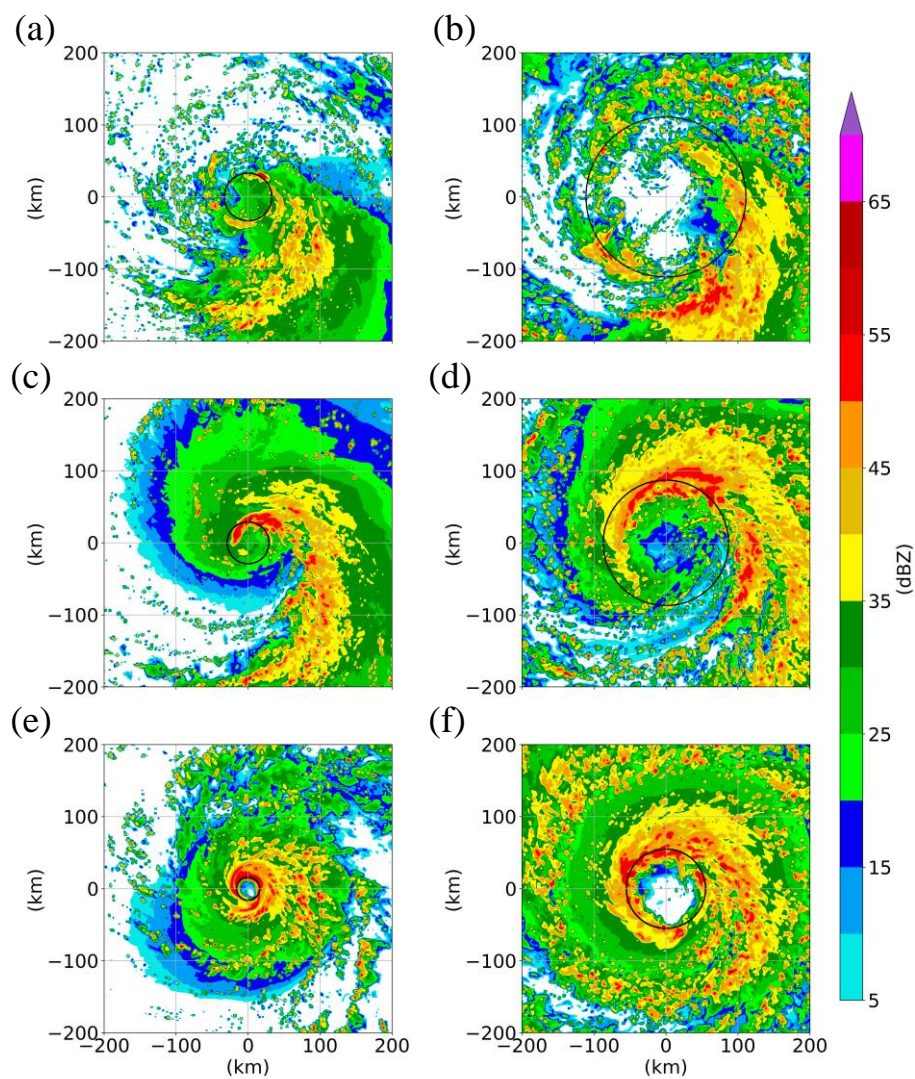
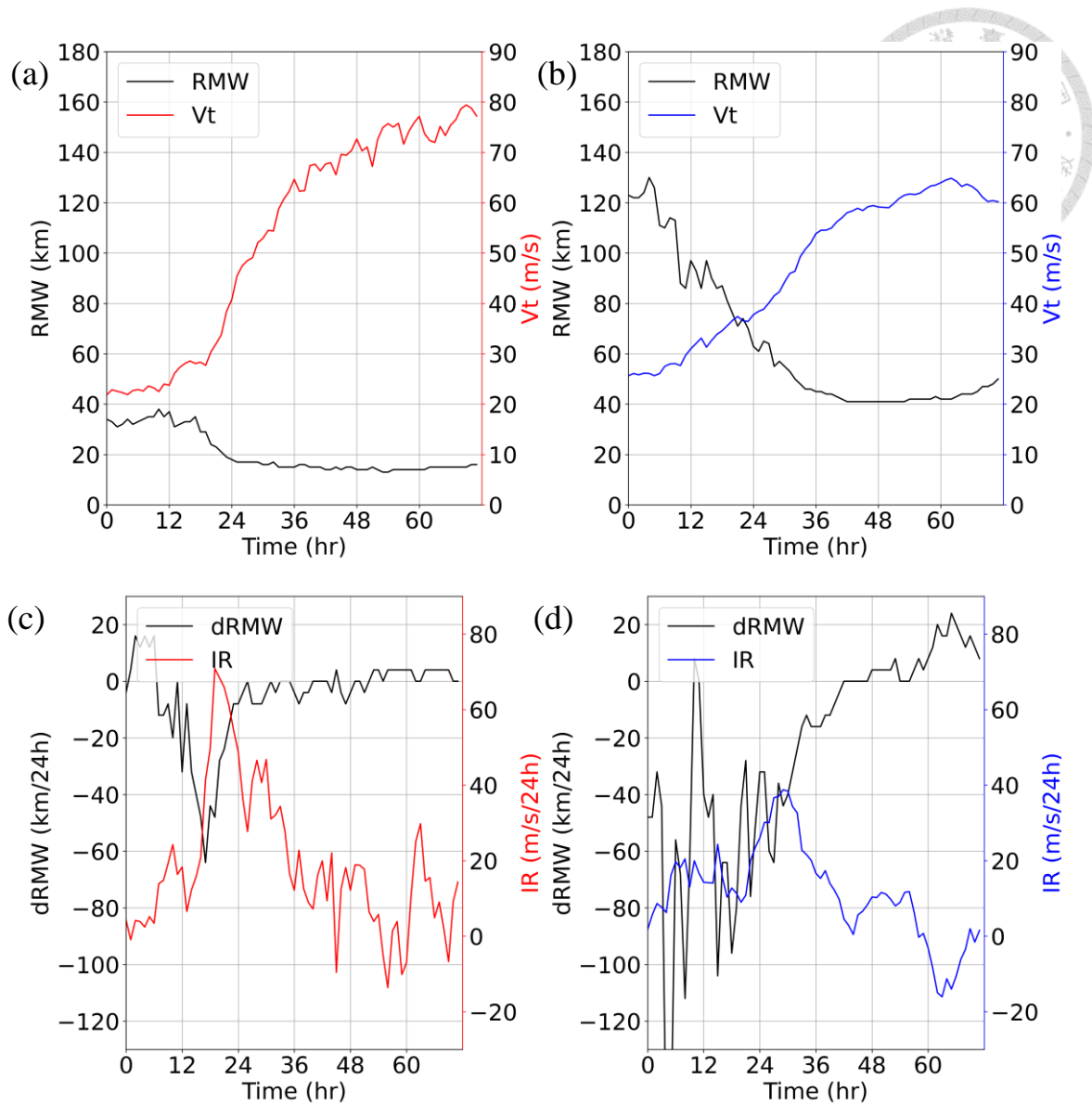Figure 4.6 Similar to Fig. 4.4, but for model-derived reflectivity (shaded). Black circle shows the RMW.

Figure 4.7 Time series of (a) and (b): RMW and maximum tangential wind speed (Vt), (c) and (d): RMW change rate (dRMW) and intensification rate of Vt (IR) of EW and MD experiments.
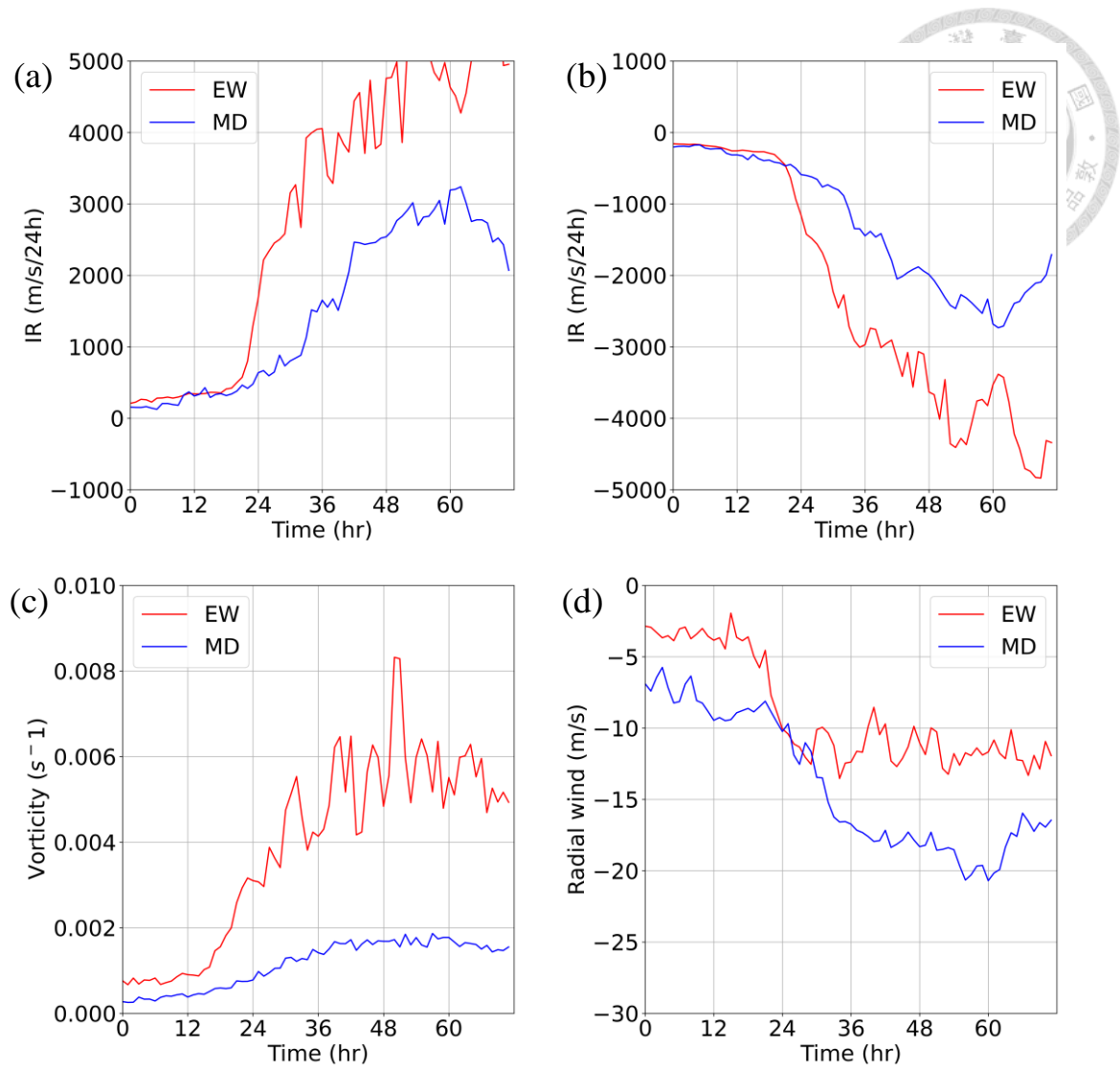
Figure 4.8 Time series of (a) positive contribution term, (b) negative contribution term of the tangential wind tendency equation at the RMW, (c) absolute vorticity, and (d) radial wind of EW and MD experiments.
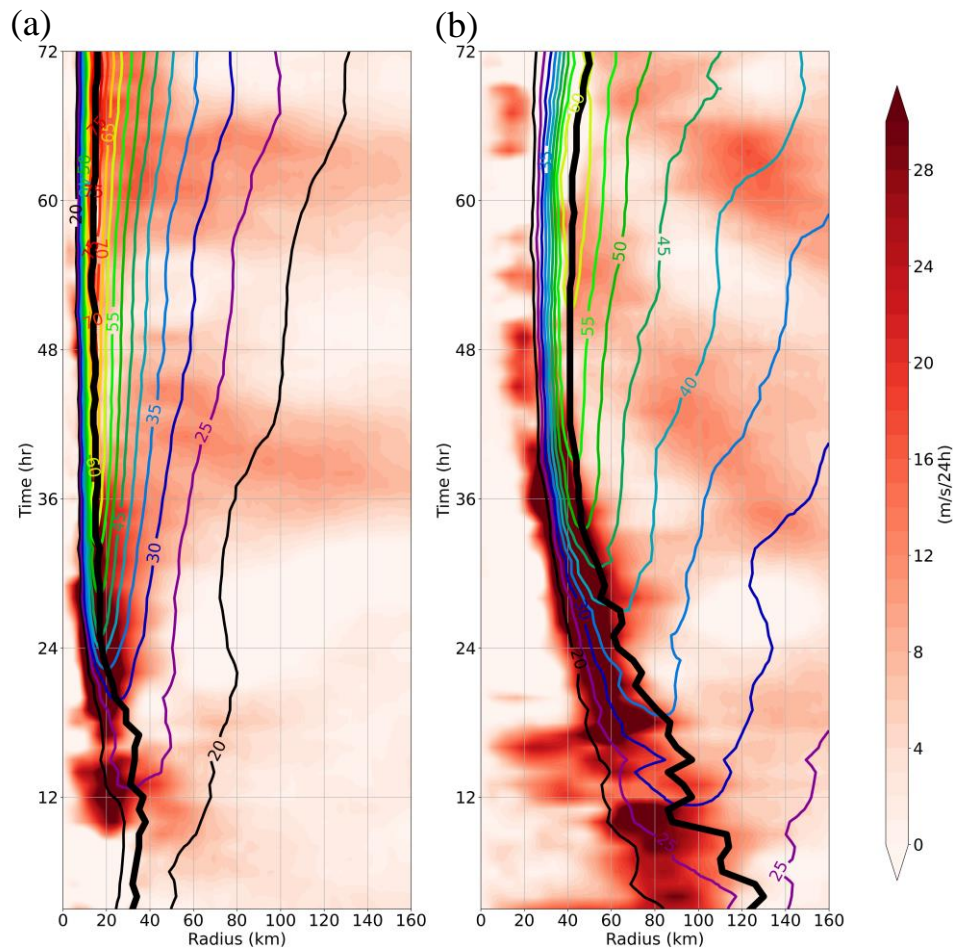
Figure 4.9 Hovmöller diagram of tangential wind speed (shaded) and change rate of tangential wind speed (contour) of (a) EW and (b) MD experiments. Black bold line shows the RMW.
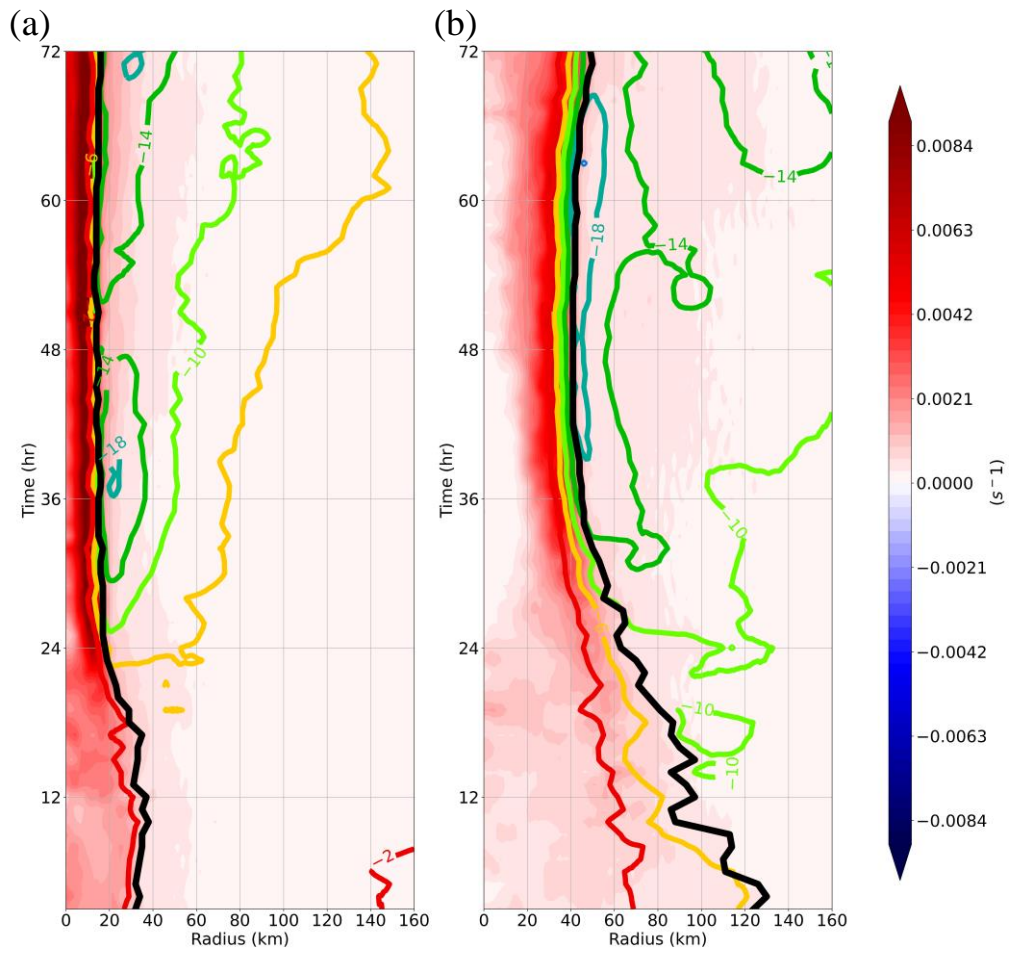
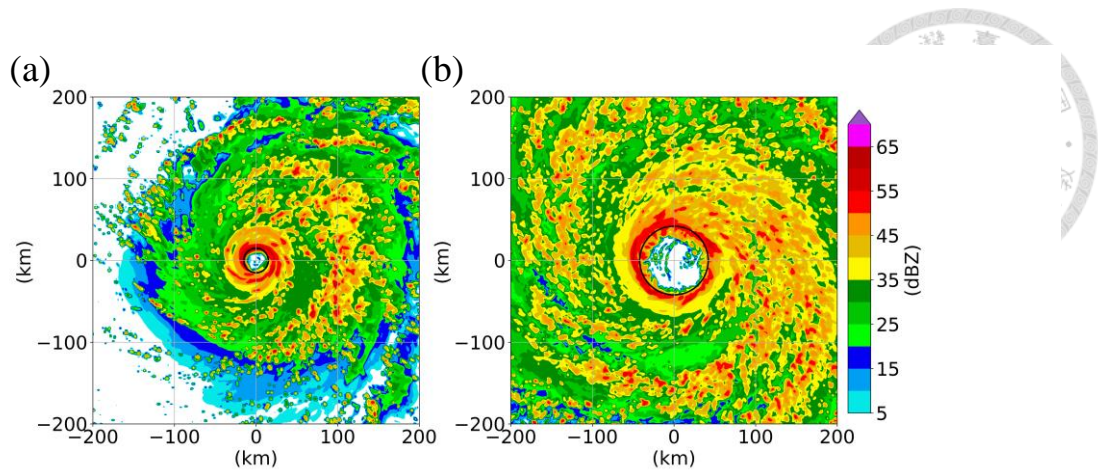Figure 4.10 Similar to Fig. 4.9, but for vorticity (shaded) and radial wind.

Figure 4.11 Model-derived reflectivity (shaded) and RMW (black circle) in (a) EW at the 36 h, and (b) MD at the 60 h.
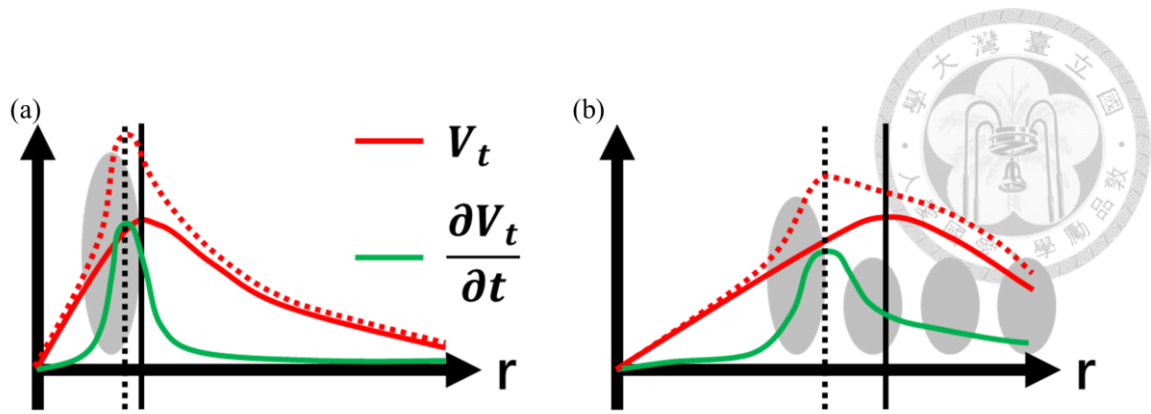
Figure 5.1 The schematic diagram of the RMW contraction and intensification process in (a) EW, and (b) MD referenced from Wu and Ruan (2021). The black lines show the RMW before (solid) and after (dashed) the diabatic heating process (shaded).